Colloids and Surfaces A: Physicochemical and Engineering Aspects 686 (2024) 133190

Contents lists available at ScienceDirect

Colloids and Surfaces A: Physicochemical and Engineering Aspects

journal homepage: www.elsevier.com/locate/colsurfa

Preparation, characterization, adsorptive and antimicrobial properties of Fe_3O_4@SiO_2@ZnO nanocomposite

Elijah Yanda Shaba [a,b,*], Jimoh Oladejo Tijani [a,b], John Olusanya Jacob [a], Mohammed Abubakar Tanko Suleiman [a], John Tsado Mathew [c]

[a] Department of Chemistry, Federal University of Technology, P. M. B. 65, Minna, Niger State, Nigeria
[b] Nanotechnology Research group, Africa Centre of Excellence and Food Safety, Federal University of Technology, P. M. B. 65, Minna, Niger State, Nigeria
[c] Department of Chemistry, Ibrahim Badamasi Babangida University Lapai, Nigeria

HIGHLIGHTS

- Fe3O4@SiO2@ZnO nanocomposites prepared at different mixing ratios.
- sRemoval of COD and BOD from petroleum wastewater.
- Effect of mixing ratio on antimicrobial activity of Fe3O4@SiO2@ZnO nanocomposites.
- Recyclability of Fe3O4@SiO2@ZnO nanocomposites.

GRAPHICAL ABSTRACT

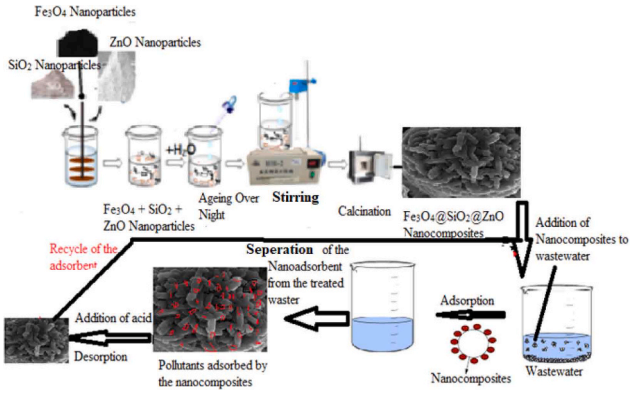

ARTICLE INFO

Keywords:
Petroleum refinery wastewater
Fe_3O_4@SiO_2@ZnO nanocomposites
Mixing ratio
Antimicrobial

ABSTRACT

A wide range of toxic contaminants, including hydrocarbons, mercaptans, phenol, ammonia and sulfide found in the wastewater from petroleum refineries have diverse health effects on human and aquatic species. In this work, the sequestration of COD and BOD from petroleum refinery wastewater by Fe_3O_4@SiO_2@ZnO nanoabsorbent prepared at different mole ratios (1:1:1, 1:1:2, 1:2:1 and 2:1:1) was carried out via the batch adsorption method. The nanomaterials synthesized by a combination of sol-gel and wet impregnation techniques were characterized using FTIR, HRSEM, EDS, XPS, XRD, DLS and BET. The HRSEM result revealed a rod-like formation with little spherical shapes on the surfaces regardless of the mixing ratios. Based on the XRD analysis SiO_2 and ZnO maintained their phases while that of Fe_3O_4 nanoparticles changed with respect to the mixing ratios. BET analysis confirmed higher surface area for Fe_3O_4@SiO_2@ZnO prepared with a mixing ratio of 1:2:1 (35.469 m^2/g) as compared to 24.918, 30.685, 15.751 m^2/g obtained for other mixing ratios (1:1:1, 1:1:2 and 2:1:1). The maximum removal efficiencies of COD and BOD at a contact time of 15 min, a dosage of 0.08 g, at 30 °C and a stirring speed of 250 rpm were 98.19% and 92.19%. The adsorption of COD and BOD at different temperatures using all the nanoadsorbent irrespective of the mixing ratios were endothermic in nature and Langmuir isotherm

* Corresponding author at: Department of Chemistry, Federal University of Technology, P. M. B. 65, Minna, Niger State, Nigeria.
E-mail address: elijah.shaba@futminna.edu.ng (E.Y. Shaba).

https://doi.org/10.1016/j.colsurfa.2024.133190
Received 20 October 2023; Received in revised form 2 January 2024; Accepted 8 January 2024
Available online 26 January 2024

and pseudo-second-order kinetic model provided the best description of the experimental data, indicating the chemical adsorption process. The regeneration studies after ten adsorption-desorption cycles indicated that the adsorbent could successfully remove COD (51.06%) and BOD (45.56%). The $Fe_3O_4/SiO_2/ZnO$ nanocomposites (1:2:1) nanoparticles was found to exhibit the greatest antimicrobial activity with 29.50 mm zone of inhibition against *Salmonella typhi,* 25.00 mm, 26.00 mm zone of inhibition obtained for *Escherichia coli* and *Klebsiella pneumoniae* compared to others prepared with different mixing ratios. This study demonstrated that Fe_3O_4@-SiO_2@ZnO nanocomposites with a mixing ratio (1:2:1) possesses excellent adsorptive, antimicrobial and recyclability properties

1. Background to the study

The earnings accrue from the sales of crude oil and associated products have impacted significantly on the standard of living in many countries especially Nigeria because the country relies heavily on petrochemical sector for her revenue [1]. However, the conversion of crude oil to useful products such as gasoline, diesel, and lubricating oils often lead to generation of a large volume of wastewater that contains diverse organic and inorganic constituents such as toluene, phenols, benzene, ethylbenzene, xylene, vanadium, iron, cadmium, nickel, selenium, chromium, copper, zinc, molybdenum and cyanide, sulfur dioxide, nitrogen oxides and hydrogen sulfate [2,3]. These pollutants particularly BTEX compounds (Benzene, Toluene and Ethyl benzene, Xylene) are non-biodegradable and their presence either at low or high concentration in petroleum wastewater have been reported by researchers [4]. For instance, exposure to benzene and ethylbenzene has been associated with hematopoietic cancers and leukemia [5]. Xylene and toluene are not cancerous, however long term exposure even at low concentrations can have negative impacts on the reproductive system [6]. In addition, Liu *et al.* [7] found that xylene at high concentrations could metabolized in the liver via oxidation of methyl groups, and damage the liver. Short and long-term exposure to toluene by both animals and humans often results in distortion of the central nervous system, inflammation of upper respiratory system, dizziness, sore throat amongst [8]. Phenol and phenolic compounds are also common occurring pollutants in petrochemical industries. Phenol is highly toxic to human beings and the environment; however difficult to remove from wastewater due to its non-biodegradable nature [9]. According to reports, phenol is extremely known to be unpleasant to human mucous membranes, eyes and skin depending on length of exposures [10]. Exposure to low or high concentrations of phenols can lead to a dark coloration of the urine, anorexia, salivation, diarrheal, vertigo and progressive weight loss [11]. Even though, these pollutants exist at very low concentrations, concerns about their effect on humans, animals, and even aquatic life have continued to grow. The amount of these pollutants particularly the organic types in the petroleum refinery wastewater can be measured by determining the indicator parameters such as COD and BOD. Studies have shown that aquatic life may be at greater risk due to high levels of COD and BOD in the wastewater [12]. Therefore, the concentration of COD and BOD in petroleum wastewater must be reduced to a permissible level before being released into various water bodies.

Most of the reported conventional available methods such as coagulation, flocculation, reverse osmosis, ultrafiltration, electrocoagulation and electro dialysis currently used for the reduction of organic pollutants from petroleum refinery wastewater have several disadvantages such as complexity in terms of design, longer treatment times and involvement of higher operational costs [13]. Hence, it is necessary to develop an alternate economical, sustainable, and environmentally friendly method for the removal of COD and BOD. Due to its high effectiveness, relative safety, and simplicity, the adsorption technology platform with nanotechnology has been recognized as a viable alternative for the removal of harmful and highly recalcitrant pollutants from petroleum refinery wastewater [14]. Researchers have employed several nanodsorbents to remove inorganic and organic pollutants in wastewater [15]. The use of single metal oxide nanoparticles such as ZnO, TiO_2, MgO, Fe_3O_4, SiO_2, and ZrO_2 as either adsorbent or photocatalyst for the elimination of complex organic and inorganic compounds is very popular. However, the problems of agglomeration, poor separation after usage, non-recyclability and low efficiency limit their use for industrial application [16]. For instance, Shaba *et al.* [17] and Shaba *et al.* [18] reported the synthesis of ZnO, SiO_2 and Fe_3O_4 nanoparticles and there still exist some limitations to the reusability of the individual nanoadsorbent after the adsorption process, making the process costly [19].

In order to overcome some of the difficulties associated with the use of individual nanoparticles researchers now focus on the development of nanocomposites including bimetallic and ternary nanocomposites, which are multifunctional in nature with better advantages of high surface area and enhanced functional groups compared to the single nanoadsorbent. For instance, Fe_3O_4 @SiO_2 @ZnO nanocomposite had been synthesized and employed as a photocatalyst by various scientists including Kiziltaş *et al.* [20]. The authors reported that within 120 min, the Fe_3O_4 @SiO_2 @ZnO composite completely degraded acid blue 161 (100%), whereas ZnO nanoparticles alone only achieved 70.9% decomposition efficiency. The findings demonstrated that the photocatalytic properties were significantly improved by the modification of ZnO with SiO_2 and ZnO nanoparticles respectively. Additionally, Fe_3O_4 @SiO_2 @ZnO photocatalyst successfully removed methylene blue (MB) within 90 min under UV light exposure and the material could be used to achieve four consecutive cycles [21].

The review of the literature also shows that there is limited information on the use of nanocomposites to treat real petrochemical wastewater. The use of real petroleum wastewater is very important because simulated wastewater contains only pure pollutant while real wastewater have different pollutants generated by the industry. To the best of our knowledge, there is paucity of information on the synthesis of Fe_3O_4 @SiO_2 @ZnO nanoadsorbent using wet impregnation method involving variation of molar ratios for the treatment of petrochemical wastewater. Thus, this present work is designed to study the effect of mixing ratios of Fe_3O_4 @SiO_2 @ZnO nanocomposite on the removal of COD and BOD using real industrial wastewater for the first time. The influence of nanoadsorbent dosage, contact time, and temperature on the elimination of COD and BOD was studied via the batch adsorption process. The data from the experiment was subjected to various isotherm and kinetics models and thermodynamics studies. Additionally, the antimicrobial and antioxidant properties of the Fe_3O_4 @SiO_2 @ZnO nanocomposites at different ratios were evaluated. Regeneration and recyclability potentials of Fe_3O_4 @SiO_2 @ZnO nanoadsorbents prepared at different molar ratios were studied to determine the stability and the economic feasibility of the removal process.

2. Materials and methods

2.1. Materials

2.1.1. List of Chemicals

Ferrous ammonium sulfate (99%), Ammonium iron (II) sulfate (98%), Manganese (II) tetraoxosulphate(97%), Sodium thiosulphate (95%), Iron (III) chloride tetrahydrate (98%), were supplied by Sigma

Aldrich. While potassium iodide (98%), nitric acid (98%) and zinc nitrate hexahydrate (98%), hydrogen tetraoxosulphate (vi) acid (96%) were by Merck while potassium dichromate (98%), sodium borohydride (97%), sodium hydroxide (95%), polyvinylpyrrolidone (99%) by BDH Chemicals.

2.1.2. Collection of petroleum wastewater

The wastewater was collected from the Kaduna refinery, Kaduna State, Nigeria in January 8th 2018. The refinery is located in the Southern part of Kaduna metropolis between latitude 10º North and longitude 7º East. While kaolin was collected from Pati Shabakolo in Niger State, Nigeria.

2.2. Methods

2.2.1. Synthesis of Fe_3O_4 nanoparticles

The process of wet chemical reduction was used for the synthesis of Fe_3O_4 nanoparticles. In the case, a 250 cm^3 beaker was filled with 15 cm^3 of 2.5 M sodium borohydride ($NaBH_4$) solution, followed by drop-by-drop addition of 50 cm^3 of 0.1 M ferric chloride hexahydrate solution under vigorous stirred. Thereafter, Ferric chloride solution was added gradually, making the final mixture darker and later completely black. The addition of full ferric chloride resulted in the production of black precipitates in less than one minute. Bubbles began to form as the reaction progressed. Once the creation of bubbles stopped, the reaction was assumed to have completed, the mixture was filtered, and the Fe_3O_4 nanoparticles produced were repeatedly washed with 100% methanol, distilled water, and later dried at 100 °C for 12 h in the oven.

2.2.2. Beneficiation and metakaolinization of Pati Kaolin

The raw kaolin was pounded and crushed and then impregnated in water at a fixed ratio of 0.1 g/L overnight to remove impurities. After three hours of stirring, the kaolin/water combination was allowed to settle and, the supernatant water was poured off. The kaolin was dried at 100 °C for 12 h in the oven and then weighed. The process of converting natural clay (Kaolin) into meta-kaolin (MK) involves crushing 50 g of kaolin, sieving (80 μm), and then calcination at 800 °C for 4 h in the furnace.

2.2.3. Synthesis of SiO_2 nanoparticles from metakaolin

Approximately 50 g of the metakaolin was weighed into 250 cm^3 followed by addition of 50 cm^3 of 2 M NaOH solution. The mixture was stirred and allowed to age for 3 h and later calcined in a furnace at 500 °C for 2 h. The resulting mixture was slowly washed with distilled water, to yield a sodium silicate solution as the filtrate. The sodium silicate produced was later used for the production of SiO_2 nanoparticles through addition of 30 cm^3 of 2 M HCl solution and subsequently agitated until a gel-like solution was obtained. The gel was later filtered and then washed severally with distilled water, and the solid residue was oven dried overnight at 100 °C. and later calcined at 450 °C for 2 h.

2.2.4. Synthesis of ZnO nanoparticles

ZnO nanoparticles were synthesized via a sol-gel approach. In this method, 50 cm^3 of 0.5 M zinc nitrate hexahydrate solution was measured into 250 cm^3 beaker. The solution was placed on a magnetic stirrer and toughly stirred for 15 min after which 2 M sodium hydroxide solution was added drop by drop followed by addition of 5 cm^3 of 10% Polyvinylpyrrolidone (PVP) solution was added to the same mixture as the structural directing agent until a white gel precipitate was obtained. Thereafter, the gel-like solution was filtered and carefully washed with deionized water to remove unreacted residue species until pH of 7 was achieved. The washed sample was dried in an oven at 100 °C for 2 h and the resultant product was then calcined at 450 °C for 5 h [17].

2.2.5. Synthesis of Fe_3O_4@SiO_2@ZnO nanocomposites

The wet impregnation method described by [18] was employed for the synthesis of Fe_3O_4 @SiO_2 @ZnO nanocomposite. The mixing of Fe_3O_4, SiO_2, and ZnO nanoparticles at different ratios is in Table 1. Then, distilled water was added, the mixture was mixed for 30 min, and allowed to age for 24 h followed by drying in the oven for 2 h at 100 °C. The final product was later calcined at 450 °C for 2 h.

2.2.6. Characterization of the Fe_3O_4@SiO_2@ZnO nanocomposite

With the use of CuK α-radiation, an X-ray diffraction (XRD) apparatus (XRD-60000) was utilized to examine the crystallite size and crystal phase of the synthesized Fe_3O_4 @SiO_2 @ZnO nanocomposites. X-ray photoelectron spectroscope (XPS, XPSHI 5400, AlK (hv =1350 eV) was used for the surface oxidation states of the elements therein the samples. The elemental composition and surface morphology of Fe_3O_4 @SiO_2 @ZnO nanocomposites were analyzed using HRSEM/Energy dispersed x-ray spectroscopy (EDS); Zeiss Auriga, SCO teen, Germany. The functional groups present in Fe_3O_4 @SiO_2 @ZnO nanocomposites were determined using FTIR Perkin Elmer 4000. Micrometric analyzer NOVA 4200e BET equipment was used for the determination of the textural properties of the nanocomposite.

2.2.7. Determination of dissolved oxygen

The level of dissolved oxygen (DO) in petroleum refinery wastewater was measured using Winkler's method. Wastewater from the refinery was collected in BOD bottles, then treated with 2.0 cm^3 manganese (II) tetraoxosulphate (VI) ($MnSO_4$) and 2.0 cm^3 potassium iodide (KI). The bottles were then filled to the mark with 250 cm^3 of petroleum wastewater. The mixture was properly mixed, corked, and allowed to precipitate for a while before allowed to settle. After the dissolution of the precipitate, 2.0 cm^3 of concentrated hydrogen tetraoxosulphate (VI) acid (H_2SO_4) was added. Starch indicator was used and 203 cm^3 of wastewater was measured into a conical flask and titrated against 0.025 mol/dm^3 sodium thiosulphate. The change from blue to colourless was noticed [22]. The level of DO in the petroleum refinery wastewater was calculated according to Eq. 1.

$$DO\left(\frac{mg}{dm^3}\right) = \frac{0.08x1000x(0.025M\ x\ Vol.of\ odium\ thiosulphate}{203} \quad (1)$$

2.2.8. Determination of biological oxygen demand

A known volume (50 cm^3) of petroleum refinery wastewater was tested for dissolved oxygen (DO) on the first day, and the DO on the fifth day was reported [23]. The same procedure was used for the blank, and Eq. 2 was used to determine the BOD level.

$$BOD\left(\frac{mg}{dm^3}\right) = \frac{(D_1 - D_2) - (B_1 - B_2)x100}{\%dilution} \quad (2)$$

Where B_1 and B_2 are the DO of the blank before incubation and after incubation (mg/dm^3) respectively. D_1 and D_2 are the DO of the petroleum wastewater before incubation and after incubation (mg/dm^3).

2.2.9. Determination of chemical oxygen demand (COD)

The dichromate method developed by the American Public Health Association was used to determine the COD level of the collected wastewater [23]. 25 cm^3 of the wastewater was measured into a 250 cm^3 beaker followed by the addition of two drops of ferrous sulfate indicator. This was then titrated against ferrous ammonium sulfate as the titrant in the burette. As shown in Eq. (3), during the titration, the

Table 1
Experimental runs for Ternary hybrid Fe_3O_4 @SiO_2 @ZnO Nanocomposites.

S/No	ZnO	Fe_3O_4	SiO_2
1	1	1	1
2	2	1	1
3	1	2	1
4	1	1	2

titrant (Fe^{2+}) rapidly interacted with the Cr^{6+} in the wastewater to produce Cr^{3+} and ferric ion (Fe^{3+}):

$$3Fe^{2+} + Cr^{6+} \rightarrow 3Fe^{3+} + Cr^{3+} \quad (3)$$

The total amount of Cr^{6+} that reduced during the digestion was calculated by subtracting the final hexavalent chromium level from the starting value before titration. Equation 4 was utilized to get the COD using this difference.

$$\frac{(A - B) \times N \times 8000}{\text{volume of sample}} \quad (4)$$

Where.

A = volume (cm^3) of $FeSO_4(HN_4)_2SO_4.(HO_2)$used for the titration of the blank.

B = volume (cm^3) of $FeSO_4(HN_4)_2SO_4.(HO_2)$used for the titration of the wastewater,

N is the normality of $FeSO_4(HN_4)_2SO_4.(HO_2)$ [23].

2.2.10. Determination of organic carbon content

A known volume of the refinery wastewater (25 cm^3) and 10.0 cm^3 of 0.5 M $K_2Cr_2O_7$ solution was measured into 250 cm^3 conical flask. Then, 20.0 cm^3 of concentrated H_2SO_4 was added to the final mixture and vigorously mixed before left for 30 min to cool. After adding 100 cm^3 of distilled water, ferroin indicator drops, and ammonium iron (II) sulphate solution, the mixture was titrated until the colour turned maroon. The amount of organic carbon (%) was calculated using Eq. 5,

$$\%\text{Organic Carbon} = \frac{(B - S)X0.4N\ X0.003X100X\ F}{Mass\ of\ the\ sample} \quad (5)$$

Where B (28.1) = constant,

S = Titre value.

N = normality.

F = constant (1.33).

2.2.11. Batch adsorption experiment for the removal of COD and BOD

Erlenmeyer flasks (250 cm^3) capacities were used for different batch experiment. During the study, the effects of contact time (1, 5, 10, 15, 20 and 25 min), adsorbent dosage (0.02, 0.04, 0.06, 0.08, 0.1 to 0.12 g/ 50 cm^3), and reaction temperature (30, 40, 50, 60, 70 and 80 °C) on the elimination of COD and BOD from the petroleum refinery wastewater were examined. Except for those adsorption experiments where the influence of temperature was studied, all experiments were conducted at 35 °C. Each flask was set up on a magnetic shaker that rotated at 250 rpm. After the interaction between the adsorbent and the petroleum refinery wastewater, the flasks were taken out of the magnetic shaker, and the liquids and nanoadsorbents were separated (using Whatman filter paper 4). The level of COD and BOD in the filterate after the interaction between the adsorbents and the petroleum refinery wastewater was then determined. The percentage removal of COD and BOD and the adsorption capacity were estimated using Eqs. (6) and (7),

$$\text{Percentage}(\%)\text{Removal} = \left(\frac{C_i - C_f}{C_f}\right) \times 100 \quad (6)$$

$$qe = \frac{(C_i - C_f)X\ V}{m} \quad (7)$$

where V = volume of petroleum wastewater used for the adsorption (L), M = mass of Fe_3O_4 @SiO_2 @ZnO nanoadsorbents used for the adsorption of COD and BOD, and C_f and C_i, are the final concentration and initial concentration of COD and BOD in the petroleum refinery wastewater at time zero and t (g/L).

2.2.12. Desorption and regeneration studies

In the desorption studies, 0.5 g of the adsorbents (Fe_3O_4 @SiO_2 @ZnO nanoadsorbent at different ratios) were weighed into four different Erlenmeyer's Flask (250 cm^3) capacity containing 20 cm^3 of 0.025, 0.08, and 0.1 $moldm^{-3}$ HNO_3, the solution was placed on an orbital magnetic shaker and stirred for 15 min at speed of 100 rpm at 30 °C. After 15 min, the nanoadsorbent was separate from the aqueous solution using Whatman filter paper No 4. Eq. 8 was used to determine the percentage of COD and BOD desorbed from the surface of the nanocomposite. To examine the regeneration potentials of each of the nanoadsorbent, 0.1 $moldm^{-3}$ concentration of HNO_3 was used as a desorbing agent to remove the pollutants from the surface of the nanocomposites. The adsorption procedure was then repeated using the regenerated adsorbent.

$$\text{Percentage Desorption} = \frac{Concentration\ of\ COD\ and\ BOD\ desobed\ by\ NHO2}{initial\ concentration\ of\ COD\ and\ BOD\ adsobed\ on\ldots}\ X100 \quad (8)$$

2.2.13. Antimicrobial susceptibility test

The antimicrobial activity of Fe_3O_4 @SiO_2 @ZnO nanocomposite prepared at the mixing ratios of 1:1:1, 1:1:2 and 1:2:1 and 2:1:1 on the *E. coli, Klebsiella pneumonia and Salmonella typhi* were determined at different concentrations of the nanocomposites using Agar diffusion method [24]. This procedure involved making nutrient-rich agar medium, pouring it into Petri dishes, and then correctly labeling each dish. Five evenly spaced holes were drilled on the surface of the agar medium using a sterile cork borer (4 mm). The pores were filled with different concentrations of the nanocomposite (20, 40, 60, 80, and 100 mg/ml), which were then injected with E. *coli, Salmonella typhi, and Klebsiella pneumoniae*, respectively, and allowed to fully diffuse at room temperature. The plates were incubated for 24 h at 37 °C. The radial growth was subsequently examined after incubation and a millimeter ruler was used to measure the zones of inhibition that each bacterial strain exhibited. The experiment was repeated three times and the average results were recorded.

2.3. Data analysis

2.3.1. Adsorption isotherm

Different adsorption isotherms such as Freundlich, Langmuir, Temkin and Dubinin-radushkevich (D-R) isotherm were utilized to study the mechanisms of the adsorption between the pollutants and the nanocomposite prepared at different mixing ratios.

Table 2
The Influence of Langmuir isotherm values on Separation Factor (RL) values.

R_L	Adsorption's nature
R_L <1	Irreversible
R_L >1	Unfavourable
R_L = 1	Linear
R_L = 0	Favourable

2.3.1.1. Langmuir isotherm. Based on the Langmuir isotherm model, pollutants were adsorbed onto the monolayer of the nanoadsorbent surfaces where the adsorbent surface exhibited identical affinity for the adsorbate. The equation for the Langmuir isotherm model is shown in Eq. 9. The nature of the adsorption process in the Langmuir isotherm model is usually established using a non-dimensional constant (R_L) (see Eq. 10). The effect of R_L values on Langmuir isotherm is expressed in Table 2.

$$\frac{C_e}{q_e} = \frac{1}{q_{max} K_L} + \frac{C_e}{q_{max}} \tag{9}$$

Where K_L = constant for Langmuir Ce (mg/L) =equilibrium concentration.

qe =amount of COD and BOD adsorbed at equilibrium while qm (mg/L) =adsorption maximum.

$$R_L = \frac{1}{1 + K_L C_e} \tag{10}$$

2.3.1.2. Freundlich adsorption isotherm. According to the Freundlich adsorption isotherm, reactions between adsorbed molecules occur in a heterogeneous distribution of active sites. Eq. (11) represents the isotherm formula for the Freundlich model. The Freundlich isotherm was utilized to evaluate the nature of the adsorption between the nanocomposite and COD and BOD removal using the n value, as shown in Table 3.

$$\log q = \log K_f + \frac{1}{n} \log C \tag{11}$$

Where qe (mg/g) = amount of COD and BOD removed at equilibrium.

Ce (mg/L) = equilibrium concentration of the COD and BOD removed from the petroleum wastewater.

KF = adsorption isotherm constant for Freundlich.

1/n = intensity of Freundlich.

2.3.1.3. Temkin isotherm. Temkin assumes that the interaction causes the heat of adsorption of the molecules in the adsorbed layer to decrease linearly with molecule coverage rather than in a logarithmic manner. This indicates that as the coverage of the adsorbed layer rise, the heat of adsorption decreased. Eq. (12) displays the formula for the Temkin isotherm.

$$q_e = \frac{RT}{b} \ln K_T + \frac{RT}{b} \ln C_e \tag{12}$$

where *q*e (mg/g) = amount of COD and BOD adsorbed, *C*e ((mg/L) = equilibrium concentration of the BOD and COD, K_T (L/mg) is the constant related to the Temkin isotherm.

2.3.1.4. Dubinin-radushkevich (D-R) isotherm. The results were subjected to D-R isotherm, which assumes that the adsorption process occurred on both homogeneous and heterogeneous surfaces, to determine whether the adsorption process is chemical or physical adsorption. The equation for D-R isotherm is expressed in Eq. (13).

$$lnq_e = lnq_m - K_{D-R\varepsilon^2} \tag{13}$$

ε is Polanyi potential, k_D is a constant related to the adsorption energy, q_e is the equilibrium concentration.

Table 3
The Effect of n values on Freundlich isotherm n value.

Nature of Adsorption	n-Value
Linear	n = 1
Chemical adsorption	n>1
Physical adsorption	n<1

2.3.2. Kinetic model

Experimental data was subjected to a variety of kinetic models, including the Pseudo first order, pseudo-second order, elovich model, and intraparticle diffusion model, to determine the adsorption mechanism process of COD and BOD removal onto Fe_3O_4 @SiO_2 @ZnO nanoadsorbent.

2.3.2.1. Pseudo first order (PFO). The PFO model was used to examine the adsorptive removal of COD and BOD from the petroleum refinery wastewater using Fe_3O_4 @SiO_2 @ZnO nanoadsorbent. The PFO kinetic model presupposes that no interaction exists between the adsorbed ions and that all adsorption takes place on isolated sites. Eq. (14) presents the PFO equation.

$$\log(q_e - q_t) = \log(q_e) - \frac{K_1}{2.303} \quad x \quad t \tag{14}$$

where, q_e and q_t (mg/g) are the amount of COD and BOD removed from the petroleum refinery wastewater at equilibrium and time (*t*), respectively.

K_1 (mg/g·min)is rate constant related to the PFO kinetic model.

2.3.2.2. Pseudo second order (PSO). If the rate of adsorption is a second-order process, the PSO assummes that the adsorption between the metal ions and the nanoadsorbent is chemisorption. The rate equation is expressed in Eq. 15:

$$\frac{t}{q_t} = \frac{1}{k_2 {q_e}^2} + \frac{t}{q_e} \tag{15}$$

where, q_e and q_t (mg/g) are the amount of COD and BOD removed from the petroleum refinery wastewater at equilibrium and time (*t*), respectively. k_2 is the rate constants related to PSO kinetic models.

2.3.2.3. Intraparticle particle diffusion (IPD). The intraparticle particle diffusion, which is usually, considered pore diffusion in an adsorption process, was used to determine if the adsorption of COD and BOD from petroleum wastewater is IPD model controlled. The equation for the IPD is shown in Eq. (16).

$$q_t = k_i t^{0.5} + C \tag{16}$$

where qt = is the amount of removed COD and BOD (mg/g) at the time (t), k (mg/g·min) and C are parameters related to the IPD model.

2.3.2.4. Elovich model. Elovich's adsorption kinetics state that the interaction between the pollutant and the nanoadsorbent is governed by the chemisorption process and the Elovich kinetic model is provided in Eq. 17.

$$qt = \frac{1}{\beta} \ln \alpha\beta - \frac{1}{\beta} \ln(t) \tag{17}$$

where qt = is the amount of removed COD and BOD (mg/g) at time (t), β (g/mg) =constant related to desorption which is associated to the chemical adsorption while α (mg/ g min1) is constant related to adsorption rate.

2.3.3. Thermodynamics studies

Fundamental thermodynamic functions utilized to determine the spontaneity and feasibility of the adsorption process between the nanoadsorbent and the target pollutants are shown in Eqs. 18–20.

$$\Delta G^o = -RT \ln K_d \tag{18}$$

$$\ln K_d = \frac{\Delta H^o}{R} - \frac{\Delta S^o}{RT} \tag{19}$$

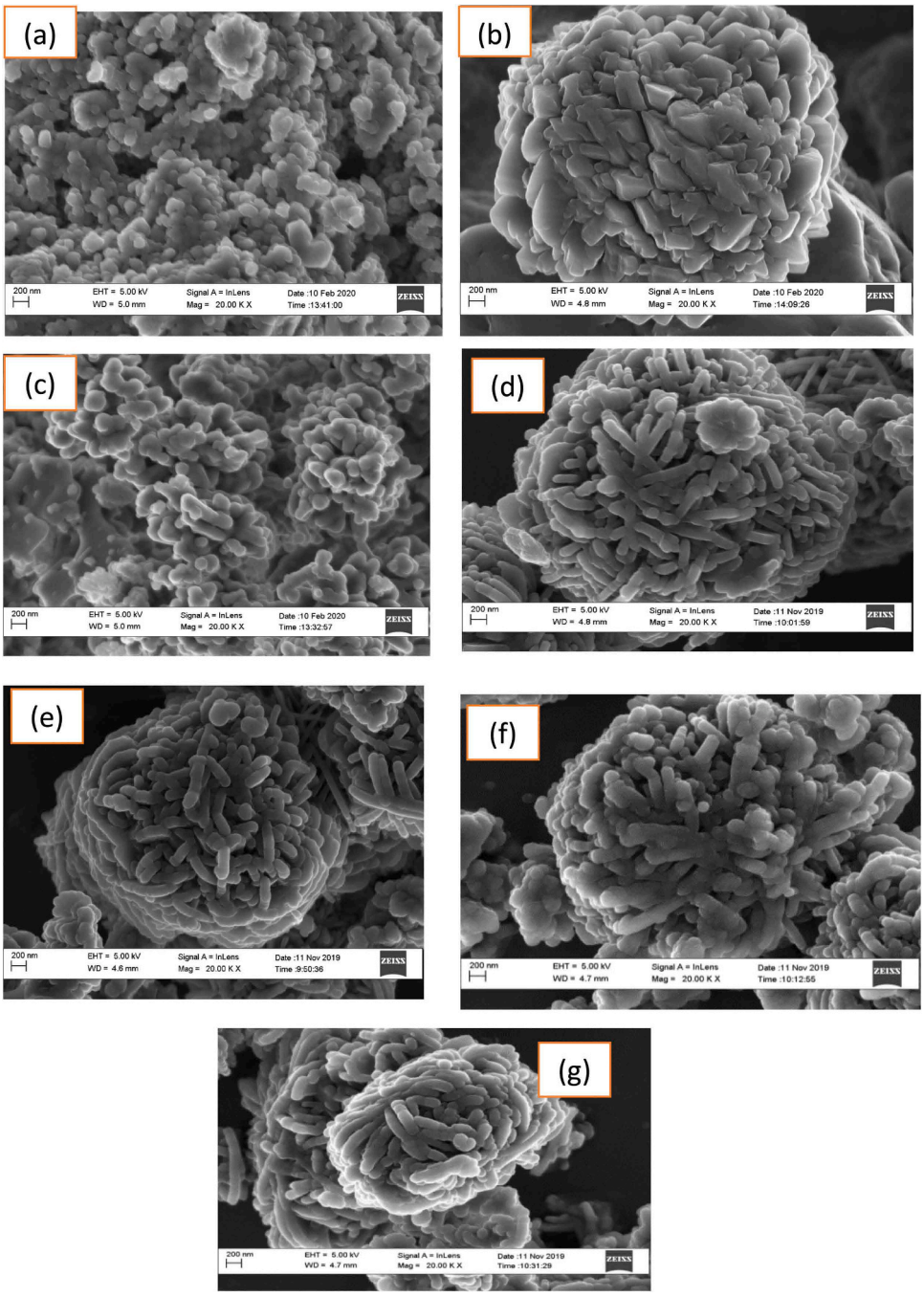

Fig. 1. HRSEM Micrographs of (a)Fe_3O, (b)SiO_2, (c)ZnO, and Fe_3O_4 @SiO_2 @ZnO Nanocomposites with Mixing Ratio (d) 1:1:1 (e) 1:1:2, (f)1:2:1 and (g) 2:1:1.

$$\Delta G^{\circ} = \Delta H^{\circ} - T\Delta S^{\circ} \quad (20)$$

Where (ΔG°, ΔH° and ΔS° are standard Gibb's free energy, entropy and standard enthalpy changes of reaction.

3. Results and discussion

3.1. HRSEM analysis of Fe_3O_4@SiO_2@ZnO nanocomposites and particle size distribution

HRSEM was utilized to examine the surface morphology of the pure Fe_3O_4, SiO_2, ZnO and Fe_3O_4 @SiO_2 @ZnO nanocomposite prepared at different mixing ratios and their corresponding micrographs are displayed in Fig. 1. Additionally, the particle size distribution histogram for Fe_3O_4 @SiO_2 @ZnO nanocomposite are presented in Fig.S2 (supplementary data).

Fig. 1(a) shows the formation of agglomerated spherical shape while Fig. 1(b) indicates compacted pyramidal shape morphology for pure SiO_2 while the pure ZnO have compacted spherical shape. Additionally, after the formation of the Fe_3O_4 @SiO_2 @ZnO nanocomposite in Fig. 1 (d), (e), (f) and (g) there was transformation from a spherical shape and pyramid shape into a fused and highly compacted rod-like shape of the Fe_3O_4 @SiO_2 @ZnO nanocomposites regardless of the ratios of the pure nanoparticles (Fe_3O_4, SiO_2 and ZnO) used. Fig. 1(d), (e), and (g) show that the Fe_3O_4 @SiO_2 @ZnO nanocomposites produced at the ratios (d) 1:1:1 (e) 1:1:2 and (g) 2:1:1 of Fe_3O_4, SiO_2 and ZnO nanoparticles were more compacted and denser compared to the Fe_3O_4 @SiO_2 @ZnO composites produced at the mixing ratios of 1:2:1 (see Fig. 1(f)). The

agglomeration may be due to the adherence of Fe_3O_4 and ZnO nanoparticles to one another by weak attractive forces resulting in (sub) micron-sized entities. It has been reported that the agglomeration of these nanoparticles reduces the chemical and mechanical characteristics of nanocomposites during their application [25]. Additionally, the agglomeration of the nanocomposites may be ascribed to the small amount of SiO_2 in the composition of the Fe_3O_4 @SiO_2 @ZnO nanocomposites at the mixing ratio of 1:1:1, 1:1:1 and 2:1:1. This suggests that the incorporation of high amount of SiO_2 nanoparticles into the lattice structure of Fe_3O_4 @ZnO nanocomposite could reduce the agglomeration. This justifies that SiO_2 is a potential material that can be used to solve the problem of agglomeration as usually associated with nanoparticles when dispersed in an aqueous medium. Additionally, the observed trend can be ascribed to the fact that SiO_2 nanoparticles are not very soluble in water and stable in both acidic and basic medium. Fritz *et al.* [26] have also demonstrated that the incorporation of SiO_2 nanoparticles onto graphene oxide increases the stability of the nanocomposites compared to the graphene oxide alone. To further understand the morphology of the Fe_3O_4 @SiO_2 @ZnO nanocomposites synthesized. HRSEM of lower magnifications are provided in the supplementary data in Fig. S2 (a), (b), (c) and (d) for the Fe_3O_4 @SiO_2 @ZnO nanocomposites synthesized at the mixing ratio of (s1) 1:1:1 (s2) 1:1:2, (s3)1:2:1 and (s4) 2:1:1 respectively. The result also shows a compacted rod-like shape in groups except for the Fe_3O_4 @SiO_2 @ZnO nanocomposites prepared 1:1:1 (s1) and 1:2:1(s3) that were not isolated from each other. Additionally, the Fe_3O_4 @SiO_2 @ZnO nanocomposites prepared at 1:1:1 (s1) was more agglomerated compared to the Fe_3O_4 @SiO_2 @ZnO nanocomposites prepared at 1:2:1 (s1). This result also confirmed the earlier conclusion that the Fe_3O_4 @SiO_2 @ZnO nanocomposites prepared at 1:2:1 is less agglomerated compared to the other ratio.

The statistical distributions of Fe_3O_4 @SiO_2 @ZnO nanocomposite with mixing ratio (a) 1:1:1 (b) 1:1:2, (c) 1:2:1 and (d) 2:1:1 derived from the HRSEM images are shown in Fig. S2. The mean particle size distribution is visible and estimated to be 95, 100, 77 and 104 nm for the Fe_3O_4 @SiO_2 @ZnO nanocomposites prepared at (a) 1:1:1 (b) 1:1:2, (c) 1:2:1 and (d) 2:1:1 respectively. This result is in agreement with the XRD result in Section 3.3.

3.2. EDS analysis of ternary Fe_3O_4, SiO_2, ZnO and Fe_3O_4@SiO_2@ZnO nanocomposites

EDS was used to analyze the Fe_3O_4, SiO_2, ZnO and Fe_3O_4 @SiO_2 @ZnO nanocomposite for the elemental composition, and the results are shown in Fig.S3 (supplementary data).

Fig.S3 reveals that the dominant elements in the ternary metallic oxide composites were Fe, Si, Zn, and O while Na was detected as impurities. Na emanated from the sodium hydroxide used for the production of the nanoparticles. According to Fig. S3, the percentage concentration of Fe was 48.94%, 13.33%, 16.03%, 50.55%; Si was 0.35%, 21.86%, 0.44%, 0.52%; Zn was 20.30%, 16.27%, 64.74%, 7.80% while O was quantified to be 30.34%, 45.77%, 18.77%, 41.13% for Fe_3O_4 @SiO_2 @ZnO with mixing ratio (d) 1:1:1 (e) 1:2:1, (f) 1:1:2 and (g) 2:1:1 respectively.

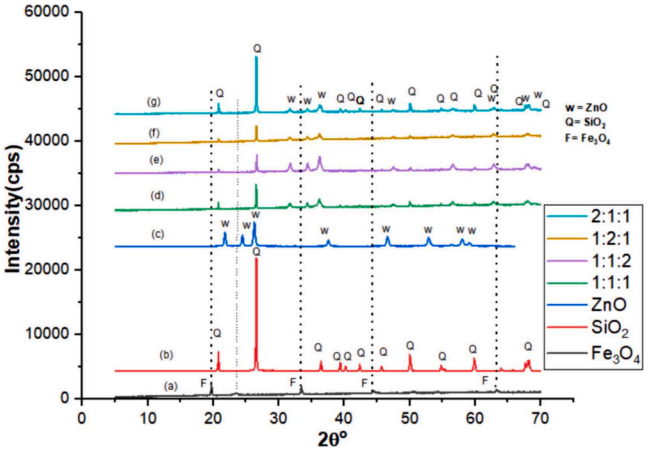

Fig. 2. XRD Patterns of Fe_3O_4 @SiO_2 @ZnO Nanocomposites prepared at (a) Fe_3O_4, (b)SiO_2, (c)ZnO (d) 1:1:1 (e) 1:1:2, (f) 1:2:1 and (g) 2:1:1.

3.3. XRD analysis of ternary Fe_3O_4@SiO_2@ ZnO nanocomposites

XRD was utilized to investigate the crystallographic structure of Fe_3O_4, SiO_2, ZnO and the Fe_3O_4 @SiO_2 @ZnO nanocomposites prepared at different mixing ratios, and the corresponding result is given in Fig. 2.

Fig. 2(a) displays the XRD spectra of pure and Fe_3O_4 nanoparticles. The diffraction peaks, which correspond to the miller indices of (220), (311), (222), (400), (422), (511), (440), (531) and (622), were observed at 2 thetha values of 27.43°, 31.65°, 35.42°, 45.51°, 54.01°, 56.44°, 62.66° and 75.28°. This matches to the face-centered cubic phase of Fe_3O_4 nanoparticles (JCP2_19–0629). The crystallite size was calculated to be 26.36 nm using Debye Scherrer's equation (see Eq. 18). Fig. 2(b) displays the XRD patterns of the synthesised SiO_2 nanoparticles. The synthesized SiO_2 nanoparticles diffractograms (Fig. 2(b)) show that the crystal planes of [100], [101], [110], [012], [111], [200], [021], [112], [202], [103], [211], [113], [212], [301] and [014] are correspondingly allocated to the diffractogram peaks at $2\theta = 20$, 26, 36, 39, 40, 42.39°, 45.71°, 50, 54, 55, 59, 63, 67, 68, and 73°. The diffraction peaks under analysis demonstrated a good agreement with the conventional cristobalite phase of SiO_2 nanoparticles (JCP2_39–1425), indicating that the crystallographic system was tetragonal in shape. Furthermore, the absence of the other peaks indicates that the SiO_2 nanoparticles synthesized is pure and devoid of impurities. This finding is a confirmation that SiO_2 nanoparticles can be synthesized from a locally available kaolin.

As seen in Fig. 2(c), the XRD diffraction pattern has nine peaks, appearing at various 2 thetha values. These correspond to ZnO nanoparticles with hexagonal wurtzite phase (JCPDS Card No. 01–089-0510). The Zn atoms occupy half of the tetrahedral sites and O atoms are organized in a hexagonal close-packed form in ZnO crystallizes in the wurtzite structure. Since the atoms of Zn and O are tetrahedrally coordinated, their positions are equal. All octahedral and half of the tetrahedral sites are unoccupied, indicating that the zinc structure is open.

Fig. 2(d), (e), (f) and (g) displays the XRD patterns of Fe_3O_4 @SiO_2 @ZnO nanocomposites with peaks at 2θ values of 21.14°, 26.96°, 37.05°, 39.91°, 40.82°, 43.05°, 46.42°, 50.77°, 55.59°, 55.95°, 60.83°, 64.83°, 66.78°, and 68.71°, corresponding to the miller planes of (100), (011), (110), (102), (111), (200), (021), (112), (202), (013), (121), (113), (300), and (212). These match well with the hexagonal cristobalite of SiO_2 (JCP2_39–1425). This suggests the stability and dominance of the SiO_2 nanoparticles after the incorporation of ZnO and Fe_3O_4 nanoparticles. In addition, the 2θ values of 31.77°, 34.42°, 36.25°, 47.53°, 56.60°, 62.86°, 67.96°, and 72.562°; correspond to (100), (002), (101), (102), (110), (103), (112), and (004) plane of the hexagonal wurtzite structure of ZnO nanoparticles, suggesting the existence of the ZnO phase after the development of the nanocomposite (JCP2–36 −1451). The 2θ values are similar to the 2θ values reported by [25] after the formation of Fe_3O_4 @ZnO@C nanocomposites. However, the 2θ values corresponding to the ZnO nanoparticles in Fe_3O_4 @SiO_2 @ZnO nanocomposites shifted to a higher diffraction peak (2θ) compared to the XRD result of the pure ZnO nanoparticles reported by [18]. The shift in the 2θ values to a higher diffraction peak suggests a decrease in crystallite size after the formation of the Fe_3O_4 @SiO_2 @ZnOnanocomposites due to the micro-strain and distortion of the crystal structure causing changes in the diffraction patterns [27]. The shift to a higher diffraction peak may be linked to the diffusion of the elements with a smaller atomic radius into the lattice structure of the

other elements [28].

There are no peaks related to Fe_3O_4 nanoparticles from the XRD results due to the absorption, shielding effects, or magnetic properties of Fe_3O_4. A related finding has been reported by Jusin *et al.* [29] who synthesized graphene-based magnetic at Fe@RGO (1:1) and Fe@RGO (1:4) ratios. The authors reported complete disappearance of peaks corresponding to magnetic nanoparticles. Taufiq *et al.* [30] also reported the disappearance of peaks corresponding to Fe_3O_4 in Silica-magnetite composites. However, Ghasemy-Piranloo *et al.* [31] synthesized Fe_3O_4 @SiO_2 @ZnO nanocomposite material with cubic magnetic cores and reported the disappearance of the peaks corresponding to the SiO_2 nanoparticles. The presence or absence of any peak of interest may be ascribed to the quantity of Fe_3O_4 or SiO_2 nanoparticles in the composite matrix.

Fig. 2(g) 2:1:1 displays highly intense diffraction peaks compared with Fig. 2(d) 1:1:1, (e) 1:1:2 and (f) 1:2:1, due to the high dosage of SiO_2 in the composites. Similarly, the higher-intensity peaks observed in Fig. 2(g) at 2θ value of 37.05° (101) plane relative to Fig. 2(d), (e) and (f) may be ascribed to high dosage of Fe_3O_4 nanoparticles in the composites of Fe_3O_4 @SiO_2 @ZnO, signifying an increase in the degree of crystallinity. This phenomenon may be linked to a higher ionic radius of Fe^{2+} (0.76 Å) than the ionic radius of Zn^{2+} (0.74 Å), leading to compression strain and ultimately increasing the unit cell of the ZnO nanoparticles when compared to the pure ZnO nanoparticle [32]. The shift in the 2θ value to high diffraction peaks may also be linked to the changes in stoichiometric composition by doping [33].

Debye Scherrer's equation (see Eq. 21) was used to estimate the average crystallite sizes of Fe_3O_4 @SiO_2 @ZnO nanocomposites and the average crystallite size was established to be equal to 10.10 nm, 8.84 nm 7.66 nm and 12.40 nm for material with mixing ratios (d) 1:1:1 (e) 1:1:2 (f) 1:2:1, and (g) 2:1:1 respectively. This suggests that the crystallite size of ternary Fe_3O_4 @SiO_2 @ZnO nanocomposites prepared at a 1:2:1 mixing ratio was the smallest and are expected to have higher surface area and be a potential adsorbent for the elimination of COD and BOD from petroleum wastewater than others

$$D = \frac{k\lambda}{\beta\cos\theta} \tag{21}$$

where D = crystallite size of the Fe_3O_4 @SiO_2 @ZnO nanocomposites β = Full width at half maximum (FWHM) of the diffraction plane, k = is constant (0.9) and λ = wavelength (1.54 Å).

3.4. Dynamic light scattering (DLS) analysis of individual Fe_3O_4, SiO_2, and ZnO nanoparticles and ternary Fe_3O_4@SiO_2@ZnO nanocomposites prepared at different mixing ratios

To determine the average size of the Fe_3O_4, SiO_2, and ZnO nanoparticles and ternary Fe_3O_4 @SiO_2@ZnO nanocomposite prepared at different mixing ratios, Dynamic light scattering (DLS) technique were used and the results are presented in Fig. S4 (supplementary data).

The average particle size of (a) Fe_3O_4, (b) SiO_2, and (c) ZnO in Fig. S4 were found to be 94.59, 80. 10 and 76.80 nm, which indicates a greater agglomerated region and poor dispersion in the liquid medium compared to the result of the DLS of 48.70, 37.60, 43.15 and 65.07 nm obtained for the Fe_3O_4 @SiO_2@ZnO prepared at mixing ratios (d) (1:1:1), (e) (1:1:2), (f) 1:2:1 and (g) 2:1:1 respectively. This result corroborated the HRSEM/ XRD results. The high value obtained for the DLS for the Fe_3O_4 @SiO_2/ZnO prepared at (2:1:1) compared to the values of Fe_3O_4 @SiO_2@ZnO prepared at (d) (1:1:1),(e) (1:1:2) and (f) 1:2:1, may be due to the high agglomeration of Fe_3O_4 @SiO_2@ZnO prepared at mixing ratio (2:1:1). This is also because DLS measures the entire size of the agglomerated structures as if they were a single molecule.

3.5. BET analysis of ternary Fe_3O_4@SiO_2@ZnO Nanocomposites

Fe_3O_4 @SiO_2 @ZnO nanocomposite textural properties (surface area, pore volume and pore diameter) were determined using the BET method; and the results are presented in Fig. S5 (supplementary data). The adsorption isotherm is divided into Types I, II, III, and IV according to IUPAC classification. All the four samples in Fig. S5 (a1) 1:1:1, (b1) 1:1:2, (c1) 1:2:1, and (d1) 2:1:1) exhibited Type IV isotherm which correspond to a mesoporous material, according to the IUPAC. The hysteresis loops occurred at a relative pressure of 0.8–1.5, as shown in Fig. S5(a) with a mixing ratio of 1:1:1. Fig. S5 (b) 1:1:2 measured have a relative pressure of 0.68–1.8. Hysteresis loops for (c) 1:2:1 were captured in the relative pressure range of 0.5–0.98. Hysteresis loops for (c) 1:2:1 were captured in the relative pressure range of 0.5–0.98. The results indicate that as the relative pressure increases, the volume of nitrogen adsorption rises until a limit is reached, which is an indication of availability of pores and binding sites [34]. Fig. S5 (a2) shows the BET and the pore diameter (inserted) for Fe_3O_4 @SiO_2 @ZnO (1:1:1). The result indicates that Fe_3O_4 @SiO_2 @ZnO (1:1:1) has a surface area, pores diameter and pore volume of ratios of 24.918 m^2/g, 0.00611 cm^3 /g and 11.32 nm. Fig. 4(b2) with a mixing ratio of 1:1:2 had a surface area, pores diameter and pore volume of 30.685 m^2/g, 0.166 cm^3 /g and 15.00 nm. The surface area, pore diameter and pore volume for Fe_3O_4 @SiO_2 @ZnO with mixing ratio 1:2:1 were 35.469 m^2/g, 0.220 cm^3 /g and 3.191 nm (Fig. S5 (c2)). Also, in Fig. S5(d2) the surface area, pore diameter and pore volume are 15.751, 0.095 and 3.581 nm respectively (see Table 4). According to Table 4, the pore diameter for nanocomposite prepared at a mixing ratio of 1:1:1, 1:1:2, 1:2:1 and 2:1:1 was less than 50 nm, an evidence of mesoporosity in the synthesized material. It was noticed that Fe_3O_4 @SiO_2 @ZnO prepared with a mixing ratio (1:2:1) has the largest surface area (35.469 m^2@g) followed by 24.918, 30.685, 15.751 m^2/g obtained for the Fe_3O_4 @SiO_2 @ZnO with mixing ratios 1:1:1, 1:1:2, 1:2:1 and 2:1:1 respectively. The increase in surface area may be linked to the increase in the amount of the SiO_2 nanoparticles, suggesting the availability of more binding sites. High surface area materials are beneficial for adsorption studies because they offer more active sites for adsorbate-adsorbent interaction. The values of the internal and external surface obtained during the adsorption-desorption isotherms suggest that the adsorption of the nanocomposites favoured the inter adsorption which is usually related to chemisorption.

3.6. XPS analysis of Fe_3O_4@SiO_2@ZnO Nanocomposite

Fe_3O_4 @SiO_2 @ZnO nanocomposite were subjected to XPS analysis to ascertain the surface oxidation states of the constituent elements and the results obtained are revealed in Fig. 3.

Fig. 3(a) demonstrates the existence of peaks at a binding energy of 103.78 eV, confirming the presence of Si in SiO_2 nanoparticles. Zinc on the sample surfaces exist in the chemical state of + 2, as evidenced by peaks at 1047 and 1025.1 eV respectively. The C (1 s) peak at 285.6 eV indicates the adventitious carbon atom from the PVP used as a capping agent during the synthesis of pure Fe_3O_4 and ZnO nanoparticles. The complete diffusion of Fe onto the internal pores of SiO_2 and ZnO shells was evidence due to the absence of peaks associated with Fe. The XPS results further supported the XRD findings in Fig. 2, where very small peaks for Fe_3O_4 were observed [35].

Fig. 3(b) depicts the spectrum of Zn 2p, with peaks at 1045.63 eV and 1022.63 eV binding energies linked with Zn 2p1/2 and Zn 2p3/2 orbitals, respectively. This suggests that Zn in Fe_3O_4 @SiO_2 @ZnO nanocomposite exists only in one valence (Zn^+) state as opposed to the Zn^{2+} described previously for the pure ZnO nanoparticles by [18]. Zn single valence state suggests that it formed a chemical bond with other elements in the Fe_3O_4 @SiO_2, and caused spin-spin split of Zn orbital. ZnO nanoparticles immobilized into Fe_3O_4 and SiO_2 have been changed and formed Fe_3O_4 @SiO_2 @ZnO nanocomposite via bonding, as shown by

Table 4
Fe_3O_4 @SiO_2 @ZnO Nanocomposite Surface Area, Pore Diameter and Total Pore Volume at different mixing ratio.

Sample Fe_3O_4@SiO_2@ZnO	BET Surface area (m^2/g)	Total Pore Volume (cm^3/g)	BJH pore Diameter (nm)	Internal surface area (m^2/g)	External surface area (m^2/g)
1:1:1	24.918	0.006	11.32	31.7182	25.062
1:1:2	30.685	0.166	15.00	32.439	29.718
1:2:1	35.469	0.220	3.191	39.439	30.08
2:1:1	15.751	0.095	3.581	19.414	17.710

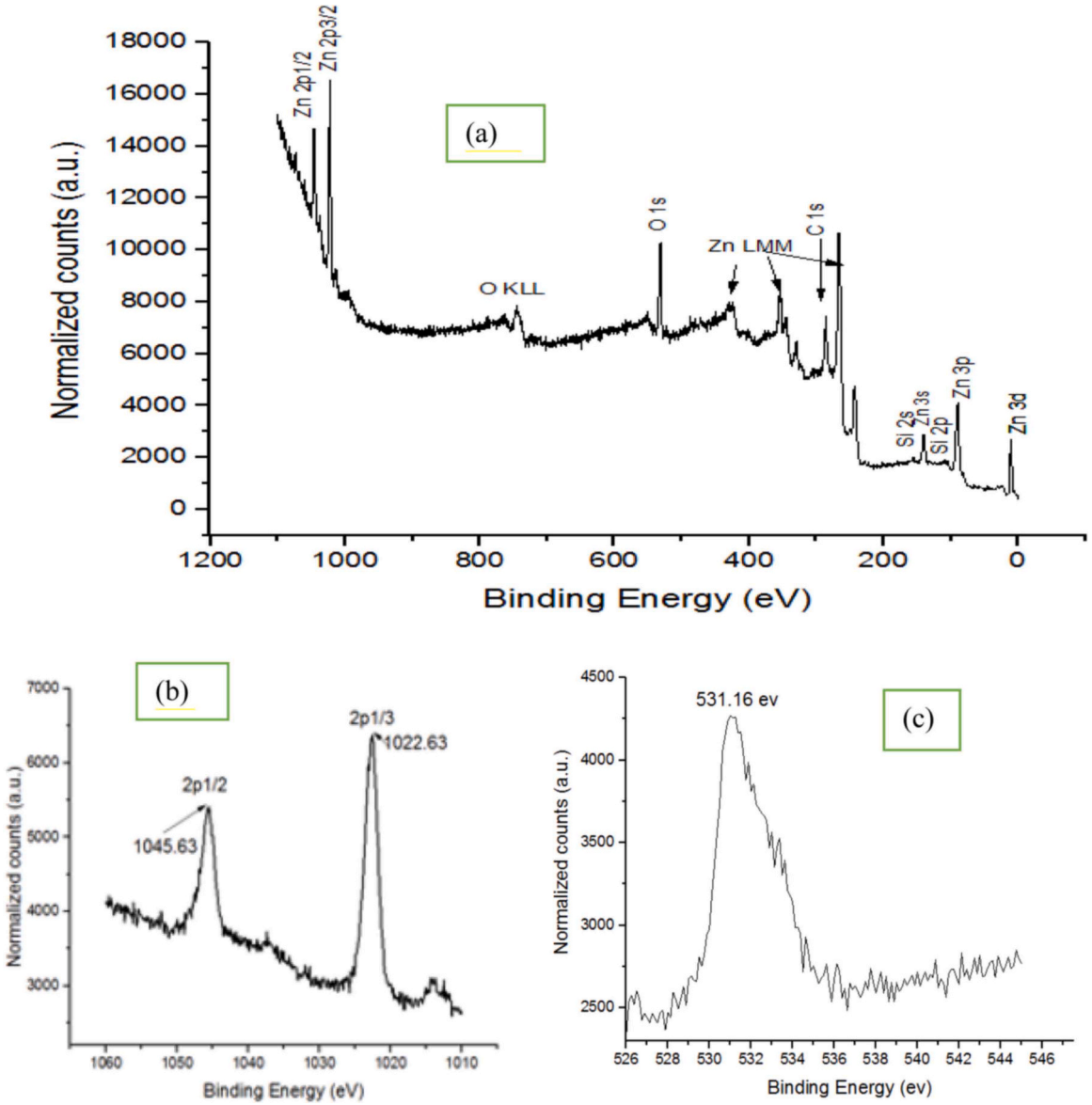

Fig. 3. (a) General XPS Survey of Fe_3O_4 @$SiO_{2@}$ZnO Nanocomposites (b) XPS Spectrum of Zn 2p3/2 (c) XPS of O (1 s) Peak in Fe_3O_4 @SiO_2 @ZnO Nanocomposites.

the two peaks in the Zn 2p XPS patterns for Fe_3O_4 @SiO_2 @ZnO nanocomposites.

XPS deconvoluted spectra of O (1 s) peak in the Fe_3O_4 @SiO_2 @ZnO nanocomposite is presented in Fig. 3(c). From the result, it can be noticed that Si-O-Si or SiO_2 like linkages exist in the Fe_3O_4 @SiO_2 @ZnO nanocomposites, as evidenced by the emergence of a peak at the binding energy of 531.16 eV. The investigation performed by multiple researchers showed peaks conforming to Si-Si, Si-OH, Al-OH, and C-O bonds [36]. The method and chemical used as precursors for the synthesis of the nanocomposites may be the cause of the discrepancy between our work and prior research.

3.7. Physicochemical characterization of the petroleum refinery wastewater

The result of the physicochemical analysis of the petroleum refinery wastewater is displayed in Table 5.

In Table 5, the pH value of 6.25 is less than the 6.51–8.5 recommended by WHO and NSDWQ. According to Orodu and Alalibo, [39], the wastewater dissolved organic carbons and carbon dioxide saturation may be responsible for the low pH. The temperature recorded is similar to the recommended values by the WHO. Insufficient dissolved air in the water due to a high temperature may result in death of aquatic

Table 5
Physicochemical Properties Raw Petroleum Refinery Wastewater Before and after Batch Adsorption Treatment with Various Nanoadsorbents.

Parameters	Concentration Before Adsorption	Concentration after adsorption				[37]WHO Permissible limits (2017)	[38]NSDQ Permissible limits (2015)
		A	B	C	D		
Chemical oxygen demand (COD) mg/L	880.15 ± 0.30	98.048 ± 0.12	74.724 ± 0.05	66.011 ± 0.05	106.586 ± 0.05	250	500
Biological oxygen demand (BOD) mg/L	190.32 ± 0.20	32.39 ± 0.05	29.328 ± 0.15	20.954 ± 0.10	44.040 ± 0.15		50
Total organic carbon (TOC) mg/L	560.12 ± 0.03	74.663 ± 0.04	62.397	51.194 ± 0.05	112.080 ± 0.10	50	40
BOD/COD ratio	0.216 ± 0.40	0.330 ± 0.05	0.392 ± 0.15	0.317 ± 0.20	0.413 ± 0.20		
Temperature (°C)	31.20 ± 0.12	31.32 ± 0.1	30.14 ± 0.12	30.04 ± 0.06	30.02 ± 0.1	31.000 ± 0.12	
pH	6.25 ± 0.10	6.34 ± 0.05	6.25 ± 0.10	7.02 ± 0.11	6.81 ± 0.11	6.34 ± 0.05	

A= Fe_3O_4 @SiO_2 @ZnO prepared at 1:1:1, B= Fe_3O_4 @SiO_2 @ZnO prepared at 1:1:2, C = Fe_3O_4 @SiO_2 @ZnO prepared at 1:2:1 and D = Fe_3O_4 @SiO_2 @ZnO prepared at 2:1:1
NSDWQ = Nigerian Standard for Drinking Water Quality and WHO = World Health Organization

organisms [40]. The value of the electrical conductivity (483.74 μS/cm) is greater than 212.00 μS/cm reported for Port Harcourt refinery wastewater by Osuoha and Nwaichi, [41]. The sample's high electrical conductivity has been linked to the presence of several dissolved ions creating a barrier for organisms' survival [42]. BOD and COD are frequently used parameters to estimate the amount of organic contamination in wastewater [43]. When compared to the WHO's recommended level of 40 mg/L, the biological oxygen demand (BOD) of wastewater from petroleum refineries is 190.32 mg/L, which is four times higher than the recommended value. This is an evidence of presence of different organic pollutants in the wastewater and low amount of oxygen to support aquatic life, and eventually may cause stress, suffocation, and even death [44]. Table 5 also shows that the COD level of petroleum refinery wastewater is 880.15 mg/L, which is lower than the 2150 mg/L reported by Mohanakrishna *et al.* [45]. The low value of the COD in this study may be linked to the nature of the wastewater. It is essential to note that the value of the COD recorded in this study is greater than the BOD level because some organic compounds in petroleum refinery wastewater may be resistant to microbial oxidation during the determination of the COD in the wastewater [46]. The BOD@COD ratio of wastewater is generally used to evaluate the possibility of an organic component breakdown in wastewater before treatment. The ratio of the BOD to COD was calculated to determine the biodegradability Index (BI) of the refinery wastewater. It has been reported that if the BI value is more than 0.6, the wastewater contains pollutants that can be biologically degraded however if the BI is between 0.3 and 0.6 physiologically methods can be applied for the wastewater treatment. However, if the BI is less than 0.3, hence the wastewater cannot be treated biologically [47]. The value of the BI (0.216 ± 0.40) obtained in this study is less than 0.3 indicating that the petroleum refinery wastewater cannot be treated by biological and physiological methods. This demonstrated that other methods are a better option for the elimination of COD and BOD from petroleum refinery wastewater rather than the use of biological or physiological methods. In this research, adsorption method was chosen over biological treatment, due to the low BOD/COD values of 0.216.

3.8. Batch adsorption studies

3.8.1. Effect of contact time

The effect of contact time on the adsorption of BOD and COD from the petroleum refinery wastewater using Fe_3O_4 @SiO_2 @ZnO nanocomposites prepared at the mixing ratios of 1:1:1, 1:1:2, 1:2:1 and 2:1:1 was studied between 1 to 25 min and the results are shown in Fig. 4(a) and (b).

Fig. 4(a) shows that the removal of COD by Fe_3O_4 @SiO_2 @ZnO nanocomposites prepared at the mixing ratios of 1:1:1, 1:1:2, 1:2:1 and 2:1:1 increase with the increase in contact time before equilibrium was attained at 20 min. The percentage (%) COD removed was 40.09%, 45.79%, 51.82% and 39.00% while the percentage (%) BOD removed was 35.09%, 40.79%, 47.82% and 30.00% after 1 min of contact time using Fe_3O_4 @SiO_2 @ZnO (1:1:1), Fe_3O_4 @SiO_2 @ZnO (1:1:2), Fe_3O_4 @SiO_2 @ZnO (1:2:1) and Fe_3O_4 @SiO_2 @ZnO (2:1:1) nanocomposite respectively. This was then gradually increases to 87.50%, 91.16%, 98.19% and 82.58% for COD and 83.20, 87.06, 90.97, 78.00%, for BOD after 15 min of contact time using Fe_3O_4 @SiO_2 @ZnO (1:1:1), Fe_3O_4 @SiO_2 @ZnO (1:1:2), Fe_3O_4 @SiO_2 @ZnO (1:2:1) and Fe_3O_4 @SiO_2 @ZnO (2:1:1) nanocomposite respectively. After which, the removal efficiency was practically constant, indicating that the adsorption was saturated after the 15 min of contact time between the nanoadsorbent and adsorbate. As the contact time increases above 15 min, the removal efficiency for both COD and BOD became constant due to the exhaustion of available sites occupied by the pollutants [48]. The findings of this research revealed that Fe_3O_4 @SiO_2 @ZnO (1:2:1) nanocomposite exhibited highest percent removal efficiency compared to Fe_3O_4 @SiO_2 @ZnO (1:1:1), Fe_3O_4 @SiO_2 @ZnO (1:1:2) and Fe_3O_4 @SiO_2 @ZnO (2:1:1) nanocomposite. The observed trend can be linked to the differences in the average crystallite size (7.66 nm) and surface area (35.469 m^2/g) of the Fe_3O_4 @SiO_2 @ZnO (1:2:1) nanocomposite compared with the average crystallite size; 10.10 nm, 8.84 nm and 12.40 nm estimated for Fe_3O_4 @SiO_2 @ZnO (1:1:1), Fe_3O_4 @SiO_2 @ZnO (1:1:2) and Fe_3O_4 @SiO_2 @ZnO (2:1:1) nanocomposites respectively. Bankole *et al.* [49] have reported the elimination of COD from electroplating wastewater occurred at an optimum contact time of 70 min against 15 min reported in this study due to the nature of the nanomaterial and the surface area.

3.8.2. Effect of adsorbent dosage

The variation of adsorbent dose (0.02, 0.04, 0.06, 0.08, 0.1 to 0.12 g) on the COD and BOD removal from petroleum refinery wastewater was examined using Fe_3O_4 @SiO_2 @ZnO nanocomposites prepared at the mixing ratios of 1:1:1, 1:1:2, 1:2:1 and 2:1:1 and the results are given in Fig. 4(c) and (d). In Fig. 4(c) and (d), the level of COD removed increased from 38.39 to 88.02, 40.01 to 90.79, 45.36 to 95.40 and 33.00 to 84.00% as the adsorbent dosage increased from 0.02 to 0.1 g. While the result of the BOD presented in Fig. 4(d) indicates that the adsorption efficiency increases from 30.39 to 84.08, 34.01 to 88.02, 39.36 to 90.30 and 24.00 to 80.00%. Regardless of the mixing ratios of the Fe_3O_4 @SiO_2

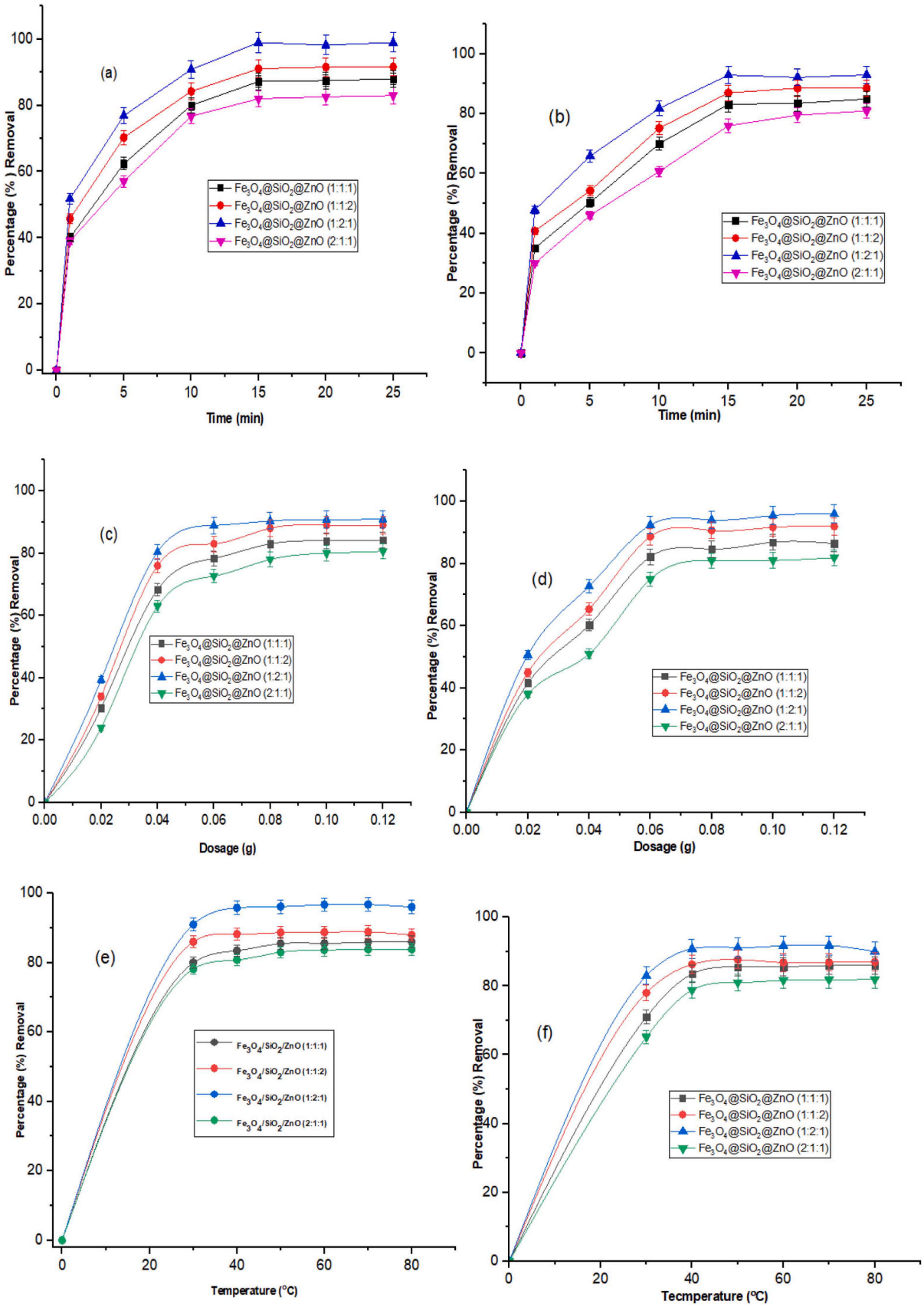

Fig. 4. Effect of Contact time on the adsorption of (a) BOD and (b) COD removal; effect of temperature on the removal of (c) COD and (d) BOD; Effect of adsorbent dosage on the removal of (e) COD and (f) BOD from petroleum refinery wastewater.

@ZnO nanocomposites, the increase in adsorption efficiency as adsorbent dosage increases suggests availability of more active sites on the nanoadsorbent surface during the COD and BOD removal. Assila et al. [50] and Dinesha et al. [51] independently reported an increase in adsorptive removal of the pollutants as a function of adsorbent dosage. Fe_3O_4 @SiO_2 @ZnO (1:2:1) nanocomposite had removal efficiency of 95.40% as against 88.02%, 90.79%, 95.40% and 84.00% obtained using Fe_3O_4 @SiO_2 @ZnO (1:1:2), Fe_3O_4 @SiO_2 @ZnO (2:1:1), Fe_3O_4 @SiO_2 @ZnO (1:1:1) nanocomposites respectively.

The rate of removal of COD and BOD in petroleum refinery wastewater was found to almost double as the dosage increased from 0.02 to 0.08 g and after 15 min. The removal efficiency became steady due to the interaction between the adsorbent and the adsorbate for the Fe_3O_4 @SiO_2 @ZnO nanocomposite prepared at 1:1:2 and 1:2:1 while Fe_3O_4 @SiO_2 @ZnO nanocomposite prepared at 1:1:1 and 1:1:2 becomes steady at 0.1 g. Almas *et al.* [52] reported a similar trend in their analysis under the reaction conditions of 0.5 to 3.0 (g L^{-1}). The steady removal of COD and BOD as the adsorbent dosage increases above 0.08 g irrespective of the mixing ratios may be ascribed to aggregation of the nanocomposite and the diffusion path length. Additionally, the high adsorption efficiency exhibited by Fe_3O_4 @SiO_2 @ZnO (1:2:1) nanocomposites compared to the other nanocomposites prepared at different mixing ratios may be linked to differences in surface area and formation of more bonds such electrostatic interactions compared with the other nanocomposites prepared at other mixing ratios [53]. The effect of adsorbent dosage on the removal of these pollutants could be explained in terms of increased coverage of the surface as the adsorbent dosage increases leading to an increase in the number of adsorption sites and enhanced removal efficiency [54].

3.8.3. Effect of adsorption temperature

The effect of temperatures (30 °C, 40 °C, 50 °C, 60 °C, 70 °C, and 80 °C) on the adsorption of COD and BOD from petroleum refinery wastewater using the four prepared nanoadsorbents were investigated, and the results are displayed in Fig. 4(e) and (f):

According to Fig. 4(e) and (f), the removal efficiency for both COD and BOD increases as the reaction temperature increases from 30 °C to 40 °C. Specifically, for COD, the adsorption rate increased from 78.00 - 83.50, 84 - 88.28, 88 - 95.82, 76.2 − 80.80% while for BOD, the amount removed increased from 71.00 - 80.50, 78 − 83.28, 83 - 90.82, 65.34 - 77.8%. The increase in adsorption rate as a function of reaction temperature suggests that the COD and BOD removal from the petroleum wastewater by the nanoadsordent is purely endothermic [54]. This corroborates the result of the thermodynamic presented in Table 6 where the value of ΔH° is positive. This result supports the findings of Zain *et al.* [55] who reported an increase in adsorption efficiency of remazol brilliant blue and malachite green dyes as the reaction temperature increases. The increment can be explained in terms of the high mobility of pollutants in the wastewater as the reaction temperature increases leading to availability of more pollutants in the wastewater having the necessary energy to engage in a surface-based interaction with active sites. In addition, rising temperature could cause the Fe_3O_4 @SiO_2 @ZnO interior structure to swell, allowing pollutants to enter into the lattice structure of the adsorbent [56]. Beyond 40 °C, the adsorption efficiency of COD and BOD from the wastewater became constant probably due to the agglomeration of the nanoadsorbent. Table 6 shows the comparison of the present study with previous works. It can be seen that when employing Fe_3O_4 @SiO_2 @ZnO (1:1:1), Fe_3O_4 @SiO_2 @ZnO (1:1:2), Fe_3O_4 @SiO_2 @ZnO (1:2:1), and Fe_3O_4 @SiO_2 @ZnO (2:1:1) nanoadsorbent, the adsorption efficiency of COD and BOD is higher. This is because majority of authors used stimulated wastewater, which contains one contaminant than the real wastewater from industries. The high or low adsorptive removal efficiency in comparison to previous studies may be due to the presence of additional pollutants in petroleum-based wastewater, which typically compete with the pollutants of interest for the active sites, as opposed to the use of stimulated wastewater that only contained the target pollutant. The variations in the adsorptive removal by the nanoadsorbent can also be attributed to the employed experimental method. In particular, in this investigation adsorption removal efficiency was achieved at 15 min compared to 20 min –2 h observed in all literature reported in Table ST1 (supplementary data). The behaviour of the nanoadsorbent could be linked to several factors such as method of synthesis, physicochemical properties of the nanomaterials, pollutants removed, and batch adsorption conditions amongst others.

3.9. Adsorption isotherm

Table ST2 (supplementary data) displays the data obtained from adsorption isotherms (Freundlich Langmuir, Temkin, and Dubinin-Rasdushkevish (D-R)) based on the batch adsorptive removal of COD and BOD from wastewater from the petroleum refinery using the four nanoadsorbents.

Table ST2 displays the findings of experimental data analyzed using several isotherm models to remove COD and BOD from wastewater from petroleum refineries. Using Fe_3O_4 @SiO_2 @ZnO nanocomposites prepared at a 1:2:1 mixing ratio, the results show that the adsorption of COD and BOD from petroleum refinery wastewater fits better to the Langmuir isotherm model due to its highest correlated coefficient (R^2) values of 0.999. These values are higher than the 0.998, 0.995, and 0.976 recorded for Freundlich, Temkin, and D-R isotherm. For the elimination of COD and BOD from petroleum refinery effluent, different Fe_3O_4 @SiO_2 @ZnO nanocomposites made at various ratios of 1:1:1, 1:1:2, and 2:1:1 also showed a similar trend.

The Langmuir isotherm's high (R^2) value in comparison to the other isotherms shows that monolayer adsorption mechanisms dominate the adsorption process. Langmuir isotherm was best fitted, followed by Freundlich isotherm, Temkin isotherm, and then D-R isotherm. The value of maximum adsorption capacity (q_{max}) values for the removal of COD were 0.134,51.641, 58.637, and 38.912 mg/g while the maximum adsorption capacity (q_{max}) for BOD were 324.641,40.637, 49.806 and 24.134 mg/g using Fe_3O_4 @SiO_2 @ZnO nanocomposites prepared at 1:1:1, 1:1:2, 1:2:1 and 2:1:1 respectively. This result indicates that among the Fe_3O_4 @SiO_2 @ZnO nanocomposites prepared at the mixing ratio of 1:2:1 performed better than Fe_3O_4 @SiO_2 @ZnO nanocomposites prepared using other mixing ratios.

Table 6
Thermodynamic Parameters for the Adsorption of BOD and COD using Fe_3O_4 @SiO_2 @ZnO Nanocomposites Prepared at different mixing ratios.

Parameters	Nanomaterials	ΔH kJ/mol	ΔS J/K.mol	ΔG kJ/mol					
				303 K	313 K	323 K	333 K	343 K	353 K
BOD	Fe_3O_4 @SiO_2 @ZnO(1:1:1)	21.016	15.159	16.422	16.271	16.119	15.968	15.816	15.664
	Fe_3O_4 @SiO_2 @ZnO(1:1:2)	14.127	6.872	12.044	11.976	11.907	11.838	11.770	11.701
	Fe_3O_4 @SiO_2 @ZnO(1:2:1)	19.235	15.035	9.497	9.498	9.499	9.501	9.502	9.504
	Fe_3O_4 @SiO_2 @ZnO(2:1:1)	28.371	30.398	19.161	18.857	18.553	18.249	17.945	17.641
COD	Fe_3O_4 @SiO_2 @ZnO(1:1:1)	24.23	13.056	20.274	20.143	20.013	19.888	19.752	19.621
	Fe_3O_4 @SiO_2 @ZnO(1:1:2)	26.721	20.541	20.497	20.291	20.086	19.881	19.675	19.470
	Fe_3O_4 @SiO_2 @ZnO(1:2:1)	15.590	10.745	12.334	12.227	12.119	12.012	11.904	11.797
	Fe_3O_4 @SiO_2 @ZnO(2:1:1)	27.945	22.951	20.991	20.761	20.532	20.302	20.073	19.843

From the result presented in Table ST2 in the supplementary data. the values obtained for the (R_L) values ranges from 0.017 to 0.024 for COD while BOD ranges from 0.016 to 0.090, which is less than one for both COD and BOD using Fe_3O_4 @SiO_2 @ZnO prepared at different mixing ratios suggesting that the adsorption COD and BOD onto Fe_3O_4 @SiO_2 @ZnO nanocomposites were favourable (see Table 2) irrespective of the adsorbent mixing ratios used. It is significant to mentioned that the values of Fe_3O_4 @SiO_2 @ZnO prepared at the mixing ratio of 1:2:1 was lower than the values for 1:1:1, 1:1:2, 2:1:1 respectively. This indicates that the adsorption of the COD and BOD is more favourable using Fe_3O_4 @SiO_2 @ZnO nanocomposites prepared at the mixing ratio of 1:2:1. This result justifies the earlier claims that the adsorption of the COD and BOD was better using r Fe_3O_4 @SiO_2 @ZnO nanocomposites prepared at the mixing ratio of 1:2:1 compared with the Fe_3O_4 @SiO_2 @ZnO nanocomposites prepared at the mixing ratio 1:1:1, 1:1:2 and 2:1:1 respectively.

Table ST2 shows the dimensionless (R_L) values for COD and BOD, and both values were less than one, suggesting that adsorption process is advantageous especially using Fe_3O_4 @SiO_2 @ZnO nanocomposites synthesized at 1:1:1, 1:1:4, 1:2:1, and 2:1:1 as nanoadsorbent. The K_L value is a standard for the evaluation of the affinities of absorbed pollutants. The stronger the affinity between Fe_3O_4 @SiO_2 @ZnO nanocomposites and the pollutants (COD and BOD), the higher the K_L value. According to the findings, Fe_3O_4 @SiO_2 @ZnO nanocomposites prepared at 1:2:1 (6.321) had a higher affinity for the COD than those prepared at 1:1:1, 1:1:2, and 2:1:1 (2.685, 2.724, and 1.966, respectively). The data obtained for the BOD showed a similar pattern.

The Freundlich isotherm model's 1/n value was less than one for the removal of COD and BOD from petroleum refinery wastewater. This indicates that chemisorption was a key factor in the adsorption of the indicator parameters using the prepared nanoadsorbents. The higher the adsorption process, the smaller the value of 1/n. Table ST2 shows the values of parameters in the Freundlich isotherm models such as k_f (mg/g (L/mg) and 1/n which is used to justify the favourability, intensity, or surface heterogeneity between adsorbent and the adsorbate. According to Table 7, the value of (1/n) is less than one, implying that the removal of COD and BOD using Fe_3O_4 @SiO_2 @ZnO nanocomposite prepared at different mixing ratios is a typical Langmuir isotherm [54]. While value of (1/n) greater than one indicates cooperative adsorption (Freundlich isotherm). The (R^2) and R_L value suggests that the Langmuir isotherm describes monolayer adsorption of the target pollutants using Fe_3O_4 @SiO_2 @ZnO nanocomposites. Additionally, value of 1/n closer to zero implies that adsorption is less heterogeneous [57]. The presence of a positive value for B_T indicates that the adsorption was endothermic [58].

The value of (E) from the Dubinin-Radushkevich (D-R) isotherm model is used to predict the type of adsorption; E values of greater than 8 kJ/mol are often classified as chemisorption and less than 8 kJ/mol are classified as physisorption [59]. The adsorption of COD and BOD onto Fe_3O_4 @SiO_2 @ZnO nanocomposite ranges from 429.800-1215.920 kJ/mol, confirming the earlier reported dominating mechanism of chemisorption. The (E) value between 1 and 16 kJ/mol indicates that process adsorption is physisorption and chemisorption if (E) is larger than 16 kJ/mol [60]. The (E) value obtained in this study is (>>16 kJ/mol) for all Fe_3O_4 @SiO_2 @ZnO nanocomposites prepared at different ratios. This demonstrates that the adsorptive removal of COD and BOD using Fe_3O_4 @SiO_2 @ZnO nanocomposites produced at various ratios is chemisorption-based.

3.10. Adsorption kinetics

To assess the adsorption kinetics during the elimination of COD and BOD from the petroleum refinery wastewater using Fe_3O_4 @SiO_2 @ZnO nanocomposites prepared at 1:1:1, 1:1:2, 1:2:1 and 2:1:1, different kinetic models, including pseudo first, pseudo second order, Elovich kinetic and intra-particle diffusion models were employed and the results obtained are presented in Table ST3 (supplementary data).

The kinetic parameters for the Elovich, IPD, PFO, and PSO models are shown in Table ST3. Due to the greater correlation regression (R^2) value of 0.999 compared to the first-order kinetics with (R^2) in the range of (0.860–0.989), the PSO kinetic model fitted better for the elimination of COD and BOD from petroleum refinery wastewater regardless of the mixing ratio. The lower (R^2) obtained for the PFO model compared to the PSO model indicates that the PSO model is better suitable for explaining the COD and BOD adsorption behaviour onto the four nanocomposites. This also suggests that the PSO kinetic model is the rate-determining step for the adsorption of COD and BOD from petroleum refinery wastewater and that chemisorption dominated the removal process. Additionally, it was found that the (R^2) for all the nanoadsorbents was in the order of Fe_3O_4 @SiO_2 @ZnO prepared at 1:2:1 >1:1:2 > 1:1:1 > 2:1:1 nanocomposite for the target pollutants.

To ascertain the applicability of the kinetics models, the data was again subjected to the error function analysis. Lower (x^2) and SSE values for the adsorption COD and BOD utilizing different nanoadsorbents as compared to the PFO kinetic model demonstrate that the adsorption process predominantly followed the PSO kinetic model as shown in Table ST3. The result of (k_1) and (k_2) presented in Table ST3 indicates that for the COD and BOD removal, the value of (k_1) was lower than (k_2), justifying the fitness of the adsorption process to PSO than the PSO model. A similar trend was observed for the qe_1 and qe_2 as shown in Table ST2. The values of (k_1, k_2) and (qe_1 and qe_2) were in order of Fe_3O_4 @SiO_2 @ZnO (1:2:1) > Fe_3O_4 @SiO_2 @ZnO (1:1:2) > Fe_3O_4

Table 7
Antibacterial Activity of Fe_3O_4 @SiO_2 @ZnO Nanocomposites.

Samples	Bacterium	Concentration				
		20 mg/cm^3	40 mg/cm^3	60 mg/cm^3	80 mg/cm^3	100 mg/cm^3
		Zone of Inhibition (mm)				
Fe_3O_4 @SiO_2 @ZnO (1:1:1)	*Escherichia coli*	6.42 ± 0.04	8.00 ± 0.12	11.34 ± 0.06	11.00 ± ,013	15.00 ± 0.07
	Solmonella typhi	3.45 ± 0.11	6.00 ± 0.08	7.50 ± 0.14	9.20 ± 0.04	13.00 ± 0.07
	Klebsiella pneumoniae	4.40 ± 0.09	12.00 ± 0.10	15.50 ± 0.02	18.00 ± 0.01	25.00 ± 0.03
Fe_3O_4 @SiO_2 @ZnO (1:1:2)	*Escherichia coli*	11.50 ± 0.14	12.00 ± 0.10	15.00 ± 0.08	16.34 ± 0.08	18.00 ± 0.12
	Solmonella typhi	6.05 ± 0.09	7.05 ± 0.03	9.500 ± 0.06	11.00 ± 0.08	17.00 ± 0.03
	Klebsiella pneumoniae	10.15 ± 0.11	13.00 ± 0.09	17.50 ± 0.08	23.00 ± 0.23	28.50 ± 0.08
Fe_3O_4 @SiO_2 @ZnO (1:2:1)	*Escherichia coli*	14.50 ± 0.01	13.00 ± 0.07	17.80 ± 0.01	20.34 ± 0.13	25.00 ± 0.06
	Solmonella typhi	10.00 ± 0.07	14.50 ± 0.08	16.40 ± 0.10	19.00 ± 0.15	26.00 ± 0.06
	Klebsiella pneumoniae	10.42 ± 0.03	16.38 ± 0.04	20.00 ± 0.09	26.36 ± 0.03	29.50 ± 0.16
Fe_3O_4 @SiO_2 @ZnO (2:1:1)	*Escherichia coli*	4.32 ± 0.17	6.00 ± 0.012	8.45 ± 0.06	12.00 ± 0.13	15.00 ± 0.04
	Solmonella typhi	5.00 ± 0.08	6.50 ± 0.01	8.00 ± 0.03	10.350 ± 0.15	13.00 ± 0.02
	Klebsiella pneumoniae	9.00 ± 0.15	7.50 ± 0.08	9.00 ± 0.04	11.32 ± 0.03	12.00 ± 0.01
Ciprofloxacin	*Escherichia coli*	6.42 ± 0.04	8.00 ± 0.12	11.34 ± 0.06	11.00 ± ,013	15.00 ± 0.07
	Solmonella typhi	3.45 ± 0.11	6.00 ± 0.08	7.50 ± 0.14	9.20 ± 0.04	13.00 ± 0.07
	Klebsiella pneumoniae	4.40 ± 0.09	12.00 ± 0.10	15.50 ± 0.02	18.00 ± 0.01	25.00 ± 0.03

$@SiO_2$ @ZnO (1:1:1) > Fe_3O_4 $@SiO_2$ @ZnO (2:1:1) nanocomposite for both BOD and COD. This trend may be linked to the large surface area of Fe_3O_4 $@SiO_2$ @ZnO (1:2:1) compared to the other ratios as presented in Table 4.

Elovich kinetics model was further used analyse the experimental data and to better study the nature of the adsorption between the Fe_3O_4 $@SiO_2$ @ZnO prepared at different ratios and pollutants (COD and BOD) (see Table ST3). The outcome also reveals that greater value of correlation coefficient (R^2) for all of the nanoadsorbents may be associated with successful adsorption of COD and BOD from petroleum refinery wastewater. This suggests that chemical bonding was involved in the adsorption of COD and BOD on the nanoadsorbents. The values of α and β presented in Table ST3 indicate that both α and β values increase in the order of 1:2:1 > 1:1:2 > 1:1:1 > 2:1:1 for both COD and BOD. This result also justifies better performance of Fe_3O_4 $@SiO_2$ @ZnO nanocomposites prepared at 1:2:1 compared to Fe_3O_4 $@SiO_2$ @ZnO nanocomposites prepared at 1:1:2, 1:1:1 and 2:1:1 respectively.

The results were also run through the IPD model to further examine the adsorption process. The (R^2) result demonstrates that, in comparison to the PSO, Elovich, and PFO models, the IPD model has a smaller impact on the adsorption process. This discovery leads to the conclusion that many mechanisms were utilized in the adsorption of COD and BOD onto the nanoadsorbent, with chemical adsorption mechanism dominating.

3.11. Thermodynamics evaluation of adsorption of COD and BOD

The elimination of BOD and COD from petroleum refinery wastewater using Fe_3O_4 $@SiO_2$ @ZnO nanocomposites prepared at mixing ratios of 1:1:1, 1:1:2, 1:2:1 and 2:1:1 was studied using different thermodynamic parameters and the results are presented in Table 6.

All of the nanoadsorbents in Table 6 have positive values of ΔH°. This demonstrated that the adsorption of COD and BOD from petroleum refinery wastewater by the four nanoadsorbents is purely endothermic in nature. According to Table 6, the ΔS° is positive regardless of the nanoadsorbent employed and the positive value denotes a higher degree of randomness at the solution/solid interface, which can alter the structure of the adsorbate and adsorbent. The ΔG°, is a key index for the adsorption process spontaneity. The value ΔG° showed decrease as the temperature increased in respective of the mixing ratios of the nanoadsorbent, indicating an increase in the degree of spontaneity during the adsorption process. This implies that the adsorption process becomes more feasible and spontaneous as the temperature increases. Generally, the feasibility and spontaneity occurred during the adsorption process for the removal of BOD and COD onto Fe_3O_4 $@SiO_2$ @ZnO(1:1:1), Fe_3O_4 $@SiO_2$ @ZnO(1:1:2), Fe_3O_4 $@SiO_2$ @ZnO(1:2:1) and Fe_3O_4 $@SiO_2$ @ZnO(2:1:1) from petroleum refinery wastewater. This suggests that the ternary metallic oxide nanocomposite prepared at mixing ratio of 1:2:1 performed better than the other ratios. The observed trend may be ascribed to the surface area, functionality and crystallite sizes of the nanoadsorbents.

3.12. Recyclability potential of $Fe_3O_4@SiO_2@ZnO$ nanocomposites

The applied Fe_3O_4 $@SiO_2$ @ZnO nanocomposites prepared at different mixing ratios (1:1:1, 1:1:2, 1:2:1 and 2:1:1) were recycled ten times under the same conditions to study the reusability of Fe_3O_4 $@SiO_2$ @ZnO nanocomposites material and the results obtained are presented in Fig. 5(a) and (b).

Fig. 5(a) shows the regeneration efficiency of COD removal from wastewater using Fe_3O_4 $@SiO_2$ @ZnO (1:1:1), Fe_3O_4 $@SiO_2$ @ZnO (1:1:2), Fe_3O_4 $@SiO_2$ @ZnO (1:2:1) and Fe_3O_4 $@SiO_2$ @ZnO (2:1:1) nanocomposite. It was noticed that the regeneration efficiency for the COD removal from petroleum refinery wastewater for the first cycle was 84.66%, the second cycle was 83.66% the third cycle was 76.86% while the percentage removal for the fourth cycle was 74.27% using Fe_3O_4 $@SiO_2$ @ZnO (1:1:1) nanocomposite, the percentage removal efficiency decreases as the number of cycles increases up to the tenth cycles. The same trend was observed for Fe_3O_4 $@SiO_2$ @ZnO (1:1:2) nanocomposite, the removal efficiency for the first cycle was 86.99%, the second cycle was 85.24% the third cycle was 78.99% while the percentage removal efficiency for the fourth cycle was 76.02% while for the tenth cycle was 25%. The values obtained for the first, second, third, fourth, fifth, sixth, seventh, eighth, ninth and tenth cycles were 90.01%, 88.45%, 87.01%, and 85.85%, 81.03%, 77.00%, 74.09%, 60.34%, 60.00% and 51.06% using Fe_3O_4 $@SiO_2$ @ZnO (1:2:1) nanoparticles. For Fe_3O_4 $@SiO_2$ @ZnO (2:1:1) nanoparticles, the regeneration efficiency for the first cycle was 80.99%, the second cycle was 79.08%, the third cycle was 75.99% and the fourth cycle was 73.91% while for the other cycles were 64%, 56%, 44%, 34% @ 0% and 18%. The result suggests that Fe_3O_4 $@SiO_2$ @ZnO (2:1:1) nanocomposites show the lowest regeneration efficiency after the fourth cycle for the removal of COD. The same trends were observed for the removal of BOD. As the

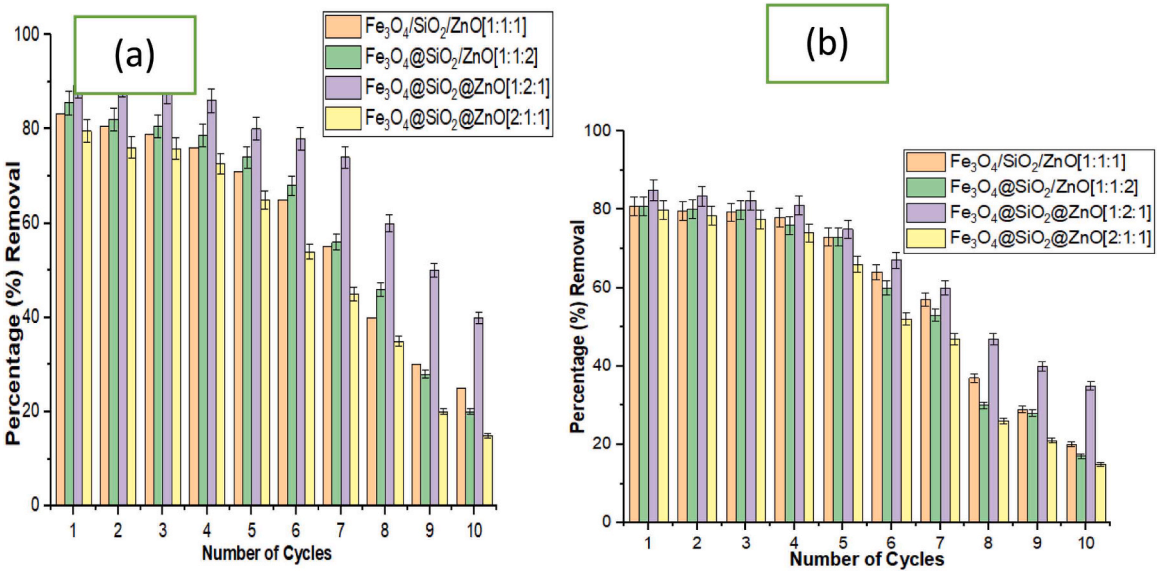

Fig. 5. Fe_3O_4 $@SiO_2$ @ZnO Nanocomposites Reusability for Adsorption of (a) COD and (b) BOD after Ten Cycles using 0.1 $moldm^{-3}$ HNO_3 Solution as the Desorption Agent.

number of cycles increases to 10 the efficiency of the nanocomposites decreases irrespective of the mixing ratio.

Generally, the regeneration efficiency of the nanocomposites followed the order of mixing ratios: 1:2:1 > 1:1:2 > 1:1:1 > 2:1:1 for both COD and BOD. This is an indication that Fe_3O_4 @SiO_2 @ZnO (1:2:1) nanocomposites were more stable than the other nanocomposites. This observation corroborated the XRD result shown in Fig. 2. It is worth noting that as the regeneration process progressed from the first to the tenth adsorption cycle, the saturation time decreased, resulting in lower adsorption removal efficiency of less than 5% from one cycle to another until after the seventh cycles for Fe_3O_4 @SiO_2 @ZnO (1:2:1) nanocomposites. The observed trend may be linked to the adsorbent structure or functional group deterioration during the desorption process [61]. Other possible explanations for the decrease in adsorption efficiency have been linked to the incomplete removal of the pollutants by desorbing acid from the surface of the adsorbent during each cycle period, contributing to the reduction of the number of available sites for the adsorption [62]. Hence, the produced nanocomposites can be reused for wastewater treatment.

3.13. XRD analysis of Fe_3O_4@SiO_2@ZnO nanocomposites after the adsorption Process

After the adsorption of the COD and BOD onto the Fe_3O_4 @SiO_2 @ZnO nanocomposite, the reused Fe_3O_4 @SiO_2 @ZnOnanocomposite was rinsed and dried in an oven and later subjected to XRD analysis to confirm their stability. The result obtained is given in Fig. 6.

Fig. 6 shows intense diffraction peaks observed at 2θ values of 20.14°, 25.96°, 36.05°, 38.91°, 39.82°, 42.05°, 45.42°, 49.77°, 54.59°,54.95°, 59.83°, 63.83°, 65.78°, and 68.771°, corresponding to the miller planes of (100), (011), (110), (102), (111), (200), (021), (112), (202), (013), (121), (113), (300), and (212) for Fe_3O_4 @SiO_2 @ZnO nanocomposites. These diffraction peaks angle and miller indices aligned with JCP2_77–001. The XRD preterm in Fig. 6 revealed a little shift (1.2°) in the peak positions and decreases in the intensity of the peaks compared with the XRD pattern of the SiO_2 @Fe_3O_4 @ZnO nanocomposite before application as presented in Fig. 2. This observation can be linked to the distortion of the lattice structure of the nanocomposites after the adsorption process. The reduction in peaks intensity signifies the contraction of the unit cell and slight loss of crystallinity. The reduction of the peaks may also be attributed to strong chemical interaction during the adsorption process based on the report of Lam *et al.* [63]. The diffraction peaks observed for Fe_3O_4 @ SiO_2 @ZnO nanocomposite (1:2:1) reduced compared to the others, due to the diffusion of ions into the lattice layer of ZnO nanoparticles leading to a more

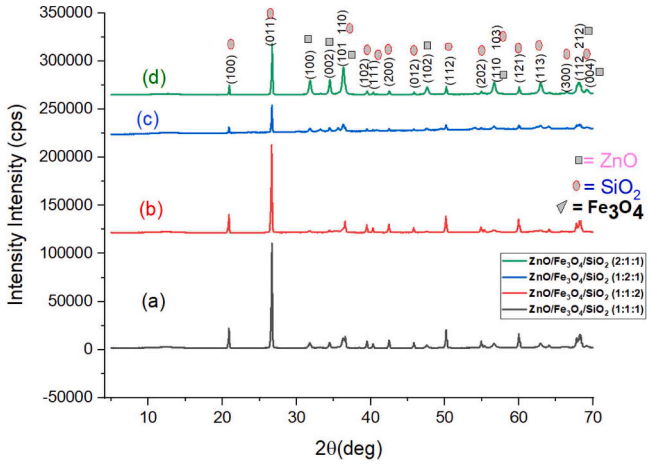

Fig. 6. XRD Patterns of Fe_3O_4 @SiO_2 @ZnO Nanocomposites after the Adsorption Process (a) 1:1:1 (b) 1:1:2, (c) 1:2:1 and (d) 2:1:1.

disordered structure of the nanocomposites after adsorption process.

Table ST4 shows that the nanoadorbent competed favourably with the results of the previous works reported in the literature. This is an indication that the nanocomposites produced in this research can be reused many times as nanodsorbent for the treatment of petroleum refinery wastewater and other related industries. Many of the researchers that utilized acid as a desorbing agent obtained higher desorption of the pollutants at 0.1 M. Other workers also employed sulphuric (H_2SO_4) acid during desorption process because of its strong oxidizing ability however sulphuric acid destroyed the active sites on the nanoadsorbents. Additionally, sulphuric acid also lead to the formation and precipitation of lead sulfate, which is insoluble in water. The percentage desorption using an alkali solution was lower compared to the use of acid solutions It can be concluded that acid had a higher desorption potential for the metal ions than base.

3.14. Antibacterial activity of Fe_3O_4@SiO_2@ZnO nanocomposites

The antibacterial properties of Fe_3O_4 @SiO_2 @ZnO nanocomposite prepared at different mixing ratios using the Agar diffusion method against the selected bacteria: *Escherichia coli*, *Klebsiella pneumonia*, and *Salmonella typhi*. were investigated. The zone of inhibition which is the area of media where bacteria are unable to grow, due to the activity of the tested nanocomposites that impedes their growth were measured in millimeters (mm) and the result is presented in Table 7 and Fig. S6, S7, S8 and S9 (supplementary data).

ST5 (the supplementary data) suggests that the nanocomposites exhibited higher antibacterial activities compared to the previous report in the literature due to the smaller crystallite size of the nanocomposites in this study. This result also justifies the claim that the crystallite size played an important role in the antibacterial activities of the nanoparticles. Fe_3O_4 @SiO_2 @ZnO (1:2:1) destroyed the cell walls of the microorganism faster than others, which suggests Fe_3O_4 @SiO_2 @ZnO (1:2:1) nanocomposites as a good antibacterial agent.

4. Conclusion

In conclusion, Fe_3O_4 @SiO_2 @ZnO nanocomposites were synthesised by wet impregnation method at different ratios. The synthesised nanocomposite were characterised using XRD, HRSEM, EDX, DLS BET and XPS in the petroleum refinery wastewater before and after the batch adsorption processes. The suitability of Fe_3O_4 @SiO_2 @ZnO nanocomposites prepared at mixing ratios of 1:1:1, 1:1:2, 1:2:1, and 2:1:1 as nanoadsorbent for the removal of BOD and COD from petroleum refinery wastewater was studied. The ternary metallic oxides (Fe_3O_4 @SiO_2 @ZnO) nanocomposites showed the formation of rod-like structures irrespective of the mixing ratio. The Fe_3O_4 @SiO_2 @ZnO (1:2:1) nanocomposites had the highest surface area of 35.469 m^2/g compared with 24.918, 30.685 and 15.751 m^2/g reported for the nanocomposites prepared at mixing ratio of 1:1:1, 1:1:2 and 2:1:1 respectively. The oxidation number of Zn^{2+} in ZnO nanoparticles changed from + 2 oxidation number to + 1 after the formation of the composites with Fe_3O_4 and SiO_2 while Fe and were + 5 (+2 and +3) and + 4 remained unchanged. The batch adsorption studies revealed the adsorptive removal efficiency of COD and BOC onto the Fe_3O_4 @SiO_2 @ZnO (1:2:1) nanocomposite prepared at different ratios. Among the ternary nanocomposites Fe_3O_4 @SiO_2 @ZnO (1:2:1) nanocomposites exhibited excellent adsorptive properties on the elimination of BOD and COD from petroleum refinery wastewater with percentage removal of 92.50% and 88.99% under the following applied conditions time (15 min), adsorbent dosage (0.08 g), reaction temperature (35 °C) and pH of 6.25. The adsorptive behaviour is directly proportional to the adsorbent's surface area and the crystallite size of the nanoadsorbent. The adsorption kinetic and isotherm models used to describe the adsorption process suggest that the adsorption process fits better to PSO kinetics than other kinetic models. While the experimental data

subjected to different isotherm models fitted best to Langmuir isotherm than others for all the adsorbents with maximum adsorptive capacity (q_{max}) of 39.806 mg/g and 36.192 mg/g for BOD and COD removal respectively. Additionally, the thermodynamics parameters showed that the adsorption process was endothermic in nature and chemisorption (chemical adsorption) controlled the adsorption process compared with the physical adsorption process. The maximum desorption of COD and BOD was 91.00% and 87. 04% at contact time (15 min), adsorbent dosage (0.08 g) and temperature of 30℃. Notably, even after the seventh adsorption cycle, the pollutant percentage removal efficiency was still over 74.09%. The stability study suggests that ZnO@SiO_2 @ Fe_3O_4(1:2:1) nanocomposite was more stable because of a slight reduction (1 - 5%) in the percentage removal of the target pollutant compared with more than 5% recorded for other composites prepared at 1:1:1, 1:12, 1:2:1and 2:1:1. Therefore, this research shows great potential of ZnO@SiO_2 @Fe_3O_4 nanocomposite for industrial wastewater treatment operations, and it may pave the way for new approach to improve sustainable nanoadsorbents for wastewater treatment and other purposes. Fe_3O_4 @SiO_2 @ZnO (1:2:1) nanocomposites exhibited the highest antibacterial activity against *Escherichia coli (*25.00 ± 0.06 nm*), Solmonella typhi (*26.00 ± 0.06 nm*), Klebsiella pneumoniae* (29.50 ± 0.16 nm) at 100 mg/. The Fe_3O_4 @SiO_2 @ZnO (1:2:1) nanocomposites have an excellent adsorptive potential to reduce the number of toxic pollutants in petroleum refinery wastewater.

Funding

This research did not receive any specific grant from funding agencies.

CRediT authorship contribution statement

Jacoba John Olusanya: Writing – review & editing, Visualization, Validation, Supervision, Software, Methodology, Funding acquisition, Formal analysis, Conceptualization. **Tijani Jimoh Oladejo:** Supervision, Resources, Project administration, Methodology, Conceptualization. **Shabaa Elijah Yanda:** Writing – review & editing, Writing – original draft, Software, Investigation, Funding acquisition, Formal analysis, Data curation, Conceptualization. **Mathew John Tsado:** Writing – review & editing, Writing – original draft, Software, Funding acquisition, Formal analysis, Conceptualization. **Suleimana Mohammed Abubakar Tanko:** Visualization, Supervision, Data curation.

Declaration of Competing Interest

The authors declare that they have no known competing financial interests or personal relationships that could have appeared to influence the work reported in this paper.

Data Availability

Data will be made available on request.

Acknowledgments

The authors appreciate the contribution of the following people for their technical assistance: Dr. Remy Bucher (XRD analysis, iThemba Labs, South Africa); Dr. Franscious Cummings (HRSEM/HRTEM/SAED/EDS) analysis, Physics department, University of the Western Cape (UWC), South Africa); and Prof. W.D. Roos for XPS analysis. Mr. Sandeeran Govender (BET analysis), Chemical Engineering Department, University of Cape Town, South Africa.

Appendix A. Supporting information

Supplementary data associated with this article can be found in the online version at doi:10.1016/j.colsurfa.2024.133190.

References

[1] O. Agbu, S.A. Nzeribe, Nigerian foreign policy and challenges of economic development, in: Nigerian Foreign Policy 60 Years After Independence, 2023, Springer International Publishing, Cham, 2023 https://link.springer.com/book/10.1007/978-3-031-06882-9.
[2] A.G. Olaremu, W.R. Adedoyin, O.T. Ore, A.O. Adeola, Sustainable development and enhancement of cracking processes using metallic composites, Appl. Petrochem. Res. 11 (1) (2021) 1–18, https://doi.org/10.1007/s13203-021-00263-1.
[3] J. Briffa, E. Sinagra, R. Blundell, Heavy metal pollution in the environment and their toxicological effects on humans, 1-20, Heliyon 6 (9) (2020), https://doi.org/10.1016/j.heliyon.2020.e0469.
[4] M. Coha, G. Farinelli, A. Tiraferri, M. Minella, D. Vione, Advanced oxidation processes in the removal of organic substances from produced water: potential, configurations, and research needs, Chem. Eng. J. 414 (2021) 128668, https://doi.org/10.1016/j.cej.2021.128668.
[5] C.J. Davidson, J.H. Hannigan, S.E. Bowen, Effects of inhaled combined Benzene, Toluene, Ethylbenzene, and Xylenes (BTEX): toward an environmental exposure model, Environ. Toxicol. Pharmacol. 81 (2021) 1–4, https://doi.org/10.1016/j.etap.2020.103518.
[6] N.A. Suaidi, M.A. Alshawsh, S.Z. Hoe, H.H. Mokhtar, S.R.M. Zin, Toxicological effects of technical xylene mixtures on the female reproductive system: a systematic review, Toxics 10 (5) (2022) 235, https://doi.org/10.3390/toxics10050235.
[7] W. Liu, S. Cao, D. Shi, L. Yu, W. Qiu, W. Chen, B. Wang, Single-chemical and mixture effects of multiple volatile organic compounds exposure on liver injury and risk of non-alcoholic fatty liver disease in a representative general adult population, Chemosphere 39 (2023) 139753, https://doi.org/10.1016/j.chemosphere.2023.139753.
[8] D.I. Ugwu, J. Conradie, Bidentate ligands in self-assembly: synthesis, structure and applications, J. Mol. Struct. (2023) 136275, https://doi.org/10.1016/j.molstruc.2023.136275.
[9] M.F. Hanafi, N. Sapawe, A review on the water problem associate with organic pollutants derived from phenol, methyl orange, and remazol brilliant blue dyes, Mater. Today.: Proc. 31 (2020) A141–A150, https://doi.org/10.1016/j.matpr.2021.01.258.
[10] S. Kuppusamy, N.R. Maddela, M. Megharaj, K. Venkateswarlu, S. Kuppusamy, N. R. Maddela, M. Megharaj, K. Venkateswarlu, Impact of total petroleum hydrocarbons on human health, Total Pet. Hydrocarb.: Environ. Fate, Toxic., Remediat. (2020) 139–165. ⟨https://link.springer.com/book/10.1007/978-3-030-24035-6⟩.
[11] V.K. Gupta, H. Karimi-Maleh, R. Sadegh, Simultaneous determination of hydroxylamine, phenol and sulfite in water and waste water samples using a voltammetric nanosensor, Int. J. Electrochem. Sci. 10 (1) (2025) 303–316, https://doi.org/10.1016/S1452-3981(23)04994-5.
[12] A.S. Mahmoud, R.S. Farag, M.M. Elshfai, L.A. Mohamed, S.M. Ragheb, Nano zero-valent aluminum (nZVAl) preparation, characterization, and application for the removal of soluble organic matter with artificial intelligence, isotherm study, and kinetic analysis, Air, Soil Water Res. 12 (2019), https://doi.org/10.1177/1178622119878707.
[13] A.D.L.M.D. Medeiros, C.J.G.D. Silva Junior, J.D.P.D. Amorim, I.J.B. Durval, A.F.D. S. Costa, L.A. Sarubbo, Oily wastewater treatment: methods, challenges, and trends, Processes 10 (4) (2022) 743, https://doi.org/10.3390/pr10040743.
[14] A.S. Ganie, S. Bano, N. Khan, S. Sultana, Z. Rehman, M.M. Rahman, M. Khan, Nanoremediation technologies for sustainable remediation of contaminated environments: recent advances and challenges, Chemosphere 275 (2021) 130065, https://doi.org/10.1016/j.chemosphere.2021.130065.
[15] J.O. Ighalo, P.S. Yap, K.O. Iwuozor, C.O. Aniagor, T. Liu, K. Dulta, K, S. Rangabhashiyam, Adsorption of persistent organic pollutants (POPs) from the aqueous environment by nano-adsorbents: a review, Environ. Res. 212 (2022) 113123 ttps://doi.org/10.1016/j.envres.2022.113123.
[16] E.Y. Shaba, J.O. Jacob, J.O. Tijani, M.A.T. Suleiman, A critical review of synthesis parameters affecting the properties of zinc oxide nanoparticle and its application in wastewater treatment, Appl. Water Sci. 11 (2021) 1–48, https://doi.org/10.1007/s13201-021-01370-z.
[17] E.Y. Shaba, J.O. Tijani, J.O. Jacob, A.A.T. Suleiman, Simultaneous removal of Cu (II) and Cr (VI) ions from petroleum refinery wastewater using ZnO/Fe3O4 nanocomposite, J. Environ. Sci. Health A Tox Hazard Subst. Environ. Eng. 57 (2022) (2022) 1146–1167, https://doi.org/10.1080/10934529.2022.2162794.
[18] E.Y. Shaba, J.O. Tijani, J.O. Jacob, A.A.T. Suleiman, Effect of mixing ratios of SiO2 nanoparticles synthesized from metakaolin on the physicochemical properties of ZnO/SiO_2 nanocomposites, Nano-Struct. Nano-Objects 35 (2023) 101003, https://doi.org/10.1016/j.nanoso.2023.101003.
[19] A.V. Baskar, N. Bolan, S.A. Hoang, P. Sooriyakumar, M. Kumar, L. Singh, T. Jasemizad, L.P. Padhye, G. Singh, A. Vinu, B. Sarkar, Recovery, regeneration and sustainable management of spent adsorbents from wastewater treatment streams: a review, Sci. Total Environ. 822 (2022) 153555, https://doi.org/10.1016/j.scitotenv.2022.153555.

[20] H. Kiziltaş, T. Tekin, D. Tekin, Synthesis, characterization of Fe3O4@ SiO2@ ZnO composite with a core-shell structure and evaluation of its photocatalytic activity, J. Environ. Chem. Eng. 8 (5) (2020) 104160, https://doi.org/10.1016/j.jece.2020.104160.

[21] F. Ghasemy-Piranloo, F. Bavarsiha, S. Dadashian, M. Rajabi, Synthesis of core/shell/shell Fe 3 O 4/SiO 2/ZnO nanostructure composite material with cubic magnetic cores and study of the photo-degradation ability of methylene blue, J. Aust. Ceram. Soc. 56 (2020) 507–515, https://doi.org/10.1007/s41779-019-00359-x.

[22] A. Carvalho, R. Costa, S. Neves, C.M. Oliveira, R.J.N. Silva, Determination of dissolved oxygen in water by the Winkler method: Performance modelling and optimisation for environmental analysis, Microchem. J. 165 (2021) *1–9*, https://doi.org/10.1016/j.microc.2021.106129.

[23] APHA, 2005. *Standard methods for the examination of water and wastewater*. 21st edition, American public health association/american water works association/water environment federation, Washington DC. 1–297. https://www.scirp.org/(S(czeh2tfqyw2orz553k1w0r45))/reference/ReferencesPapers.aspx?ReferenceID=1870039.

[24] E.A.A. Mohamed, A.M. Muddathir, M.A. Osman, Antimicrobial activity, phytochemical screening of crude extracts, and essential oils constituents of two *Pulicaria spp.* growing in Sudan, Sci. Rep. 10 (2020) 17148, https://doi.org/10.1038/s41598-020-74262-y.

[25] S. Arief, R.A. Usna, Synthesis and properties of magnetic-luminescent Fe3 O 4@ ZnO/C nanocomposites, J. Nanotechnol. (2023) *1–7*, https://doi.org/10.1155/2023/2381623.

[26] P.A. Fritz, S.C. Lange, M. Giesbers, H. Zuilhof, R.M. Boom, C.G.P. Schroën, Simultaneous silicon oxide growth and electrophoretic deposition of graphene oxide, Langmuir 35 (10) (2019) 3717–3723, https://doi.org/10.1021%2Facs.langmuir.8b03139.

[27] A.D. Prasetya, M. Rifai, H. Miyamoto, X-ray diffraction (XRD) profile analysis of pure ECAP-annealing Nickel samples, J. Phys.: Conf. Ser. 1436 (2020) 012113.

[28] S. Dolabella, A. Borzì, A. Dommann, A. Neels, Lattice strain and defects analysis in nanostructured semiconductor materials and devices by high-resolution X-ray diffraction: theoretical and practical aspects, Small Methods 6 (2) (2022) 2100932, https://doi.org/10.1002/smtd.202100932.

[29] J.W. Jusin, M. Aziz, G.P. Sean, J. Jaafar, Preparation and characterization of graphene-based magnetic hybrid nanocomposite, Malay. J. Anal. Sci. 20 (1) (2016) 149–156, https://mjas.analis.com.my/wp-content/uploads/2018/10/JashielaWani_20_1_16.pdf.

[30] A. Taufiq, A. Nikmah, A. Hidayat, S. Sunaryono, N. Mufti, N. Hidayat, H. Susanto, H, Synthesis of magnetite/silica nanocomposites from natural sand to create a drug delivery vehicle, Heliyon 6 (4) (2020) 3784, https://doi.org/10.1088/1742-6596/1436/1/012113.

[31] F. Ghasemy-Piranloo, F. Bavarsiha, S. Dadashian, M. Rajabi, M, Synthesis of core/shell/shell $Fe_3O_4/SiO_2/ZnO$ nanostructure composite material with cubic magnetic cores and study of the photo-degradation ability of methylene blue, J. Aust. Ceram. Soc. 56 (2020) (2019) 507–515, https://doi.org/10.1007/s41779-019-00359-x.

[32] M. Carofiglio, S. Barui, V. Cauda, M. Laurenti, Doped zinc oxide nanoparticles: synthesis, characterisation and potential use in nanomedicine, Appl. Sci. 10 (15) (2020) 1–43, https://doi.org/10.3390/app10155194.

[33] O. Lupan, L. Chow, L.K. Ono, B.R. Cuenya, G. Chai, H. Khallaf, S. Park, A. Schulte, A, Synthesis and characterization of Ag-or Sb-doped ZnO nanorods by a facile hydrothermal route, J. Phys. Chem. 114 (29) (2010) 12401–12408, https://doi.org/10.1021/jp910263n.

[34] S. Fu, Q. Fang, A. Li, Z. Li, J. Han, X. Dang, W. Han, Accurate characterisation of full pore size distribution of tight sandstones by low-temperature nitrogen gas adsorption and high pressure mercury intrusion combination method, Energy Sci. Eng. 9 (1) (2020) 80–100, https://doi.org/10.1002/ese3.817.

[35] E.A. Bakr, M.N. El-Nahass, W.M. Hamada, T.A. Fayed, Facile synthesis of superparamagnetic Fe_3O_4@noble metal core–shell nanoparticles by thermal decomposition and hydrothermal methods: comparative study and catalytic applications, RSC Adv. 11 (2021) 781–797, https://doi.org/10.1039/D0RA08230A.

[36] Z. Hajizadeh, F. Hassanzadeh-Afruzi, D.F. Jelodar, M.R. Ahghari, A. Maleki, Cu (ii) immobilized on Fe_3O_4@HNTs–tetrazole (CFHT) nanocomposite: synthesis, characterisation, investigation of its catalytic role for the 1,3 dipolar cycloaddition reaction, and antibacterial activity, RSC Adv. 10 (44) (2020) 26467–26478, https://doi.org/10.1039/D0RA04772D.

[37] WHO (2017). Guidelines for drinking-water quality 4th edition incorporating the 1st addendum. (https://www.who.int/publications/i/item/9789241549950).

[38] NSDWQ (2015). Nigerian Industrial Standard https://rivwamis.riversstate.gov.ng/assets/files/Nigerian-Standard-for-Drinking-Water-Quality-NIS-554–2015.Pbf., 1–28.

[39] V.E. Orodu, M.E. Alalibo, Physicochemical and heavy metal analysis of effluent water from Port Harcourt refinery depot, Nigeria, Int Aca. J. Appl. Biomed. Sci. 1 (1) (2020) 6–17, https://doi.org/10.47310/iajabms.2020.v01i01.002.

[40] Y. Zhou, K. Wang, B. Wang, Y. Pu, J. Zhang, Occupational benzene exposure and the risk of genetic damage: a systematic review and meta-analysis, BMC Public Health 20 (1) (2020) 1–11, https://doi.org/10.1186/s12889-020-09215-1.

[41] J.O. Osuoha, E.O. Nwaichi, Physicochemical characterisation of a liquid effluent from a refinery, J. Appl. Sci. Environ. Manag. 23 (10) (2019) 1779–1782, https://doi.org/10.4314/jasem.v23i10.2.

[42] Y. Meride, B. Ayenew, Drinking water quality assessment and its effects on residents health in Wondo genet campus, Ethiopia, Environ. Syst. Res 5 (1) (2016) 1–7, https://doi.org/10.1186/s40068-016-0053-6.

[43] E. Tolulope, T.O. Aniyikaiye, O.O. John, N.E. Joshua, Physico-chemical analysis of wastewater discharge from selected paint industries in Lagos, Nigeria, Int. J. Environ. Res. Public Health 16 (7) (2019) 1235, https://doi.org/10.3390/ijerph16071235.

[44] J. Xu, G. Jin, Y. Mo, H. Tang, L. Li, Assessing anthropogenic impacts on chemical and biochemical oxygen demand in different spatial scales with bayesian networks, Water 12 (1) (2020) 246, https://doi.org/10.3390/w12010246.

[45] G. Mohanakrishna, I.M. Abu-Reesh, D. Pant, Enhanced bioelectrochemical treatment of petroleum refinery wastewater with Labaneh whey as co-substrate, Sci. Rep. 10 (2020) 19665, https://doi.org/10.1038/s41598-020-76668-0.

[46] F.K. Abagale, Seasonal variation and removal of organic pollutants in wastewater using low-cost treatment technologies in Tamale metropolis, Ghana, J. Water Resour. Prot. 13 (4) (2021) 21–30, https://doi.org/10.4236/jwarp.2021.134016.

[47] P. Dhanke, S. Wagh, Treatment of vegetable oil refifinery wastewater with biodegradability index improvement. Mater. Today.: Proc. 27 (1) (2020) 181–187, https://doi.org/10.1016/j.matpr.2019.10.004.

[48] P. Lawtae, C. Tangsathitkulchai, The Use of high surface area mesoporous-activated carbon from longan seed biomass for increasing capacity and kinetics of methylene blue adsorption from aqueous solution, Molecules 26 (21) (2021) 6521, https://doi.org/10.3390/molecules26216521.

[49] M.T. Bankole, A.S. Abdulkareem, J.O. Tijani, S.S. Ochigbo, A.S. Afolabi, W.D. Roos, Chemical oxygen demand removal from electroplating wastewater by purified and polymer functionalized carbon nanotubes adsorbents, Water Resour. Ind. 18 (2017) 33–50, https://doi.org/10.1016/j.wri.2017.07.00.

[50] O. Assila, K. Tanji, M. Zouheir, A. Arrahli, L. Nahali, F. Zerrouq, A. Kherbeche, Adsorption studies on the removal of textile effluent over two natural eco-friendly adsorbents, J. Chem. 2020 (2020) 1–13, https://doi.org/10.1155/2020/6457825.

[51] B.L. Dinesha, S. Hiregoudar, U. Nidoni, K.T. Ramappa, A.T. Dandekar, S. V. Ganachari, Adsorption modelling and fixed-bed column study on milk processing industry wastewater treatment using chitosan zinc-oxide nano-adsorbent–coated sand filter bed, Environ. Sci. Pollut. Res. 30 (13) (2023) 37547–37569, https://doi.org/10.1007/s11356-022-24873-x.

[52] M. Almas, A.S. Khan, A. Nasrullah, I.U. Din, T.M. Fagieh, E.M. Bakhsh, A. Inayat, Substantial increase in adsorption efficiency of local clay-alginate beads toward methylene blue impregnated with SDS, Environ. Sci. Pollut. Res. 30 (34) (2023) 81433–81449, https://doi.org/10.1007/s11356-022-23949-y.

[53] A. Samadi, M. Xie, J. Li, H. Shon, C. Zheng, S. Zhao, Polyaniline-based adsorbents for aqueous pollutants removal: a review, Chem. Eng. J. 418 (2021) 129425, https://doi.org/10.1016/j.cej.2021.129425.

[54] E.Y. Shaba, J.O. Tijani, J.O. Jacob, A.A.T. Suleiman, Adsorptive potential of ZnO/SiO_2 nanorods prepared via the sol–gel method for the removal of Pb (II) and Cd (II) from petroleum refinery wastewater, J. Chem. Technol. Biotechnol. 97 (8) (2022) 2196–2217, https://doi.org/10.1002/jctb.7098.

[55] Zahirah Mohd Zain, Ahmed Saud Abdulhameed, Ali H. Jawad, Zeid A. ALOthman, Zaher Mundher Yaseen, A pH-sensitive surface of chitosan/sepiolite clay/algae biocomposite for the removal of malachite green and remazol brilliant blue R dyes: optimization and adsorption mechanism study, J. Polym. Environ. 31 (2) (2023) 501–518, https://doi.org/10.1007/s10924-022-02614-y.

[56] U.L. Usman, B.U. Allam, N.B. Singh, S. Banerjee, Adsorptive removal of Cr (VI) from wastewater by hexagonal boron nitride-magnetite nanocomposites: kinetics, mechanism and LCA analysis, J. Mol. Liq. 354 (2022) 118833, https://doi.org/10.1016/j.molliq.2022.118833.

[57] M.Y. Pudza, Z.Z. Abidin, A sustainable and eco-friendly technique for dye adsorption from aqueous media using waste from Jatropha curcas (isotherm and kinetic model), Desalin. Water Treat. 182 (2020) 365–374, https://doi.org/10.5004/dwt.2020.25169.

[58] X.P. Yu, Z. Zhang, L. Pu, T. Tang, F. Guo, Breast cancer overall-survival can be predicted with a 19 lncrna tissue signature, Eur. J. Gynaecol. Oncol. 42 (5) (2021) 838–843, https://www.ejgo.net/articles/10.31083/j.ejgo4205128.

[59] P.K. Singh, A. Gautam, V. Verma, P.M. Singh, S. Shivapriya, A.K. Shivalkar, S. Sahoo, A. Kumar, Green synthesis of metallic nanoparticles as effective alternatives to treat antibiotics resistant bacterial infections: a review, Biotechnol. Rep. 25 (2020) 1–13, https://doi.org/10.1016/j.btre.2020.e00427.

[60] V. Puccia, M.J. Avena, On the use of the Dubinin-Radushkevich equation to distinguish between physical and chemical adsorption at the solid-water interface, Colloid Interface Sci. Commun. 41 (2021) 100376, https://doi.org/10.1016/j.colcom.2021.100376.

[61] J. Bayuo, M.A. Abukari, K.B. Pelig-Ba, Desorption of chromium (VI) and lead (II) ions and regeneration of the exhausted adsorbent, Appl. Water Sci. 10 (7) (2020) 1–6, https://doi.org/10.1007/s13201-020-01250-y.

[62] H. Patel, Review on solvent desorption study from exhausted adsorbent, J. Saudi Chem. Soc. 25 (8) (2021) 1–11, https://doi.org/10.1016/j.jscs.2021.101302.

[63] Y. Lam, S. Fan, L. He, Y. Ho, B. Fei, J.H. Xin, Charge-controllable mussel-inspired magnetic nanocomposites for selective dye adsorption and separation, Chemosphere 300 (2022) 134404, https://doi.org/10.1016/j.chemosphere.2022.134404.